Available online at www.sciencedirect.com

ScienceDirect

Geochimica et Cosmochimica Acta 176 (2016) 96–117

Geochimica et Cosmochimica Acta

www.elsevier.com/locate/gca

Insights into chemical weathering of the upper continental crust from the geochemistry of ancient glacial diamictites

Su Li [a,b,*], Richard M. Gaschnig [b,2], Roberta L. Rudnick [b,1]

[a] School of Geosciences, China University of Petroleum (East China), Qingdao 266555, China
[b] Geology Department, University of Maryland, College Park, MD 20742-421, USA

Received 12 June 2015; accepted in revised form 12 December 2015; Available online 21 December 2015

Abstract

Glacial diamictites, with ages ranging from ~2900 to 0.01 Ma, record the changing composition of the upper continental crust through time (Gaschnig et al., 2014). Li concentrations and isotopic compositions, combined with Pb isotopic compositions, chemical index of alteration (CIA) values and relative Sr concentrations are used here to assess the degree of chemical weathering recorded in these deposits and the origin of this signature. The δ^7Li values of most of the diamictites (ranging from −3.9 to +3.5) are lower than those of mantle-derived basalts (+3.7 ± 2, 2σ), and the low δ^7Li values are generally accompanied by high CIA and low Sr/Sr* values (or Sr depletion factor, $Sr/Sr^* = Sr/(Ce^*Nd)^{0.5}$), reflecting a weathering signature that may have derived from pre-depositional, syn-depositional, and/or post-depositional weathering processes. Profiles through three glacial diamictites with relatively high CIA (a fresh road cut of the Neoproterozoic Nantuo Formation (CIA = 62–69), and drill cores through the Paleoproterozoic Timeball Hill (CIA = 66–75) and Duitschland Formations (CIA = 84–91)) do not show evidence of significant post-depositional weathering. High Th/U, reflecting loss of uranium during oxidative weathering, is seen in all Paleozoic and Neoproterozoic diamictites and a few Paleoproterozoic deposits. Pb isotopic systematics suggest that this signature was largely inherited from preexisting crust, although a subset of samples (the Neoproterozoic Konnarock, Paleozoic Dwyka, and several of the Paleoproterozoic Duitschland samples) appears to have experienced post-depositional U loss. Modern glaciomarine sediments record little weathering (CIA = 47, Sr/Sr* = 0.7, δ^7Li = +1.8), consistent with the cold temperatures accompanying glacial periods, and suggesting that limited syn-depositional weathering has occurred. Thus, the chemical weathering signature observed in ancient glacial diamictites appears to be largely inherited from the upper continental crust (UCC) over which the glaciers traversed. The strength of this weathering signature, based on the CIA, is greatest in the Mesoarchean and some of the Paleoproterozoic diamictites and is weaker in the Neoproterozoic and Phanerozoic glacial diamictites. Combining these data with data for Archean shales and other types of post-Paleoproterozoic sedimentary rocks (i.e., shales, mudstones, etc.), it appears that post-Paleoproterozoic upper continental crust experienced less intense chemical weathering, on average, than Archean and Paleoproterozoic upper continental crust.

* Corresponding author at: Building C, Department of Geology, School of Geosciences, China University of Petroleum (East China), No. 66 West Changjiang Road, Huangdao Area, Qingdao 266555, China.
E-mail addresses: lisu19870202@gmail.com (S. Li), rgaschnig3@gatech.edu (R.M. Gaschnig), rudnick@umd.edu (R.L. Rudnick).
[1] Now at Department of Earth Science, University of California, Santa Barbara, CA 93106-9630, USA.
[2] Now at School of Earth and Atmospheric Sciences, Georgia Institute of Technology, Atlanta, GA 30332, USA.

http://dx.doi.org/10.1016/j.gca.2015.12.012
0016-7037/

1. INTRODUCTION

Chemical weathering removes soluble elements from the exposed continental crust and produces secondary minerals (clays, Fe oxides and hydroxides) via incongruent weathering. It is responsible for generating the detritus that ultimately forms clastic sedimentary rocks and for releasing soluble elements that eventually precipitate as chemical sediments, which, in turn, modulates atmospheric CO_2. While chemical weathering must have impacted the composition of the continental crust over time (Rudnick, 1995), the amount of crust thus impacted is a matter of great uncertainty (e.g., Albarède, 1998; Lee et al., 2008; Liu and Rudnick, 2011), as is the question of how weathering intensity may have changed through time.

To understand the impact of chemical weathering on the continental crust, one could turn to estimates of the average composition of continental crust, which offer insights into the processes that formed and modified it. However, estimating average crustal composition is challenging given the great lithologic heterogeneity that exists within the crust. For the upper continental crust, the focus of this paper, widespread bedrock sampling campaigns have been used to estimate its major element and soluble trace element composition (e.g., Eade and Fahrig, 1973; Gao et al., 1998), whereas the geochemistry of fine-grained terrigenous sedimentary rocks (e.g., shales, loess) are commonly used to estimate the average insoluble trace element composition (Goldschmidt, 1933; Taylor et al., 1983a,b; Taylor and McLennan, 1985; Wronkiewicz and Condie, 1987; Condie, 1993). The average UCC compositions derived from widespread sampling campaigns provide evidence that chemical weathering may have impacted its composition. For example, the average concentration of Sr (a highly soluble element and one of the first to be removed during chemical weathering of silicate rocks) in bulk continental crust (BCC) is depleted relative to the insoluble REE, and compared to igneous rock types, as measured by the Sr/Nd ratio (Fig. 5 of Rudnick, 1995). Moreover, average UCC compositional estimates have lower Sr/Nd (9–13.5, Rudnick and Gao, 2003, and references therein) compared to BCC (Sr/Nd = 10–22) and to mantle-derived igneous rocks (>15, McDonough, 1990; Rudnick, 1995). However, Sr depletion in the UCC could also be due to processes such as intracrustal differentiation that leaves Sr-rich plagioclase-bearing residues or cumulates in the deep crust. Indeed, the chemical index of alteration values ($CIA = [Al_2O_3/(Al_2O_3 + CaO^* + Na_2O + K_2O)] * 100$, where CaO^* is corrected to remove the contribution of carbonate and apatite, Nesbitt and Young, 1982; McLennan et al., 1993) of average UCC (48–56, calculated from data in Table 1 of Rudnick and Gao, 2003) overlap those of igneous rocks. These observations raise the question: how significant is chemical weathering in shaping the crust's composition?

Glacial sediments provide an alternative means of assessing the average composition of the upper continental crust that may circumvent the issues associated with loss of soluble elements given that they form largely by physical weathering processes, as first suggested by Goldschmidt (1933). Although glacially derived loess often carries a chemical weathering signature (Gallet et al., 1998), Nesbitt and Young (1996) confirmed the dominance of

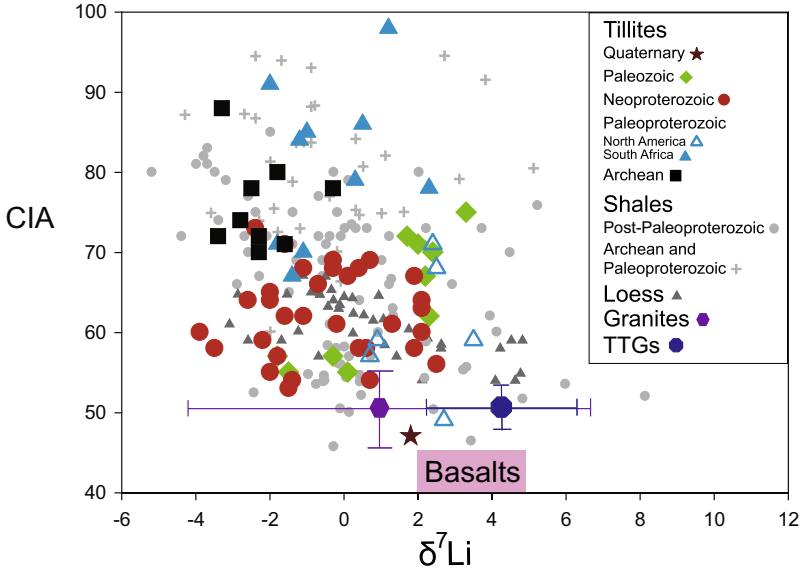

Fig. 1. δ^7Li vs. CIA in glacial diamictites, shales and loess. The glacial diamictite data are from this study whereas new data, as well as literature data for Archean and Paleoproterozoic shales are provided in Appendix Table A6-1. Post-Paleoproterozoic rocks include glacial diamictites (this study) and other sedimentary rocks (loess, shales, clay) compiled from the literature (Bouman et al., 2004; Teng et al., 2004; Chan et al., 2006; Qiu et al., 2009, 2011; Sauzéat et al., 2015; Appendix Table A6-1). The δ^7Li and CIA data for average granites are compiled from Pearce et al., 1984; Castro et al., 1999; James and Palmer, 2000; Moyen et al., 2001; Wu et al., 2002; Rudnick et al., 2004; Teng et al., 2004, 2006, 2009; Yang et al., 2004, 2006; Magna et al., 2010; Liu et al., 2010; Cuccuru et al., 2012; Huang et al., 2013a,b,c. The δ^7Li and CIA data for average TTGs are from Teng et al., 2008; Donskaya et al., 2009; Qiu, 2011; Moyen, 2011; Seixas et al., 2012; Huang et al., 2013a,b,c. The pink rectangle shows the δ^7Li average of fresh MORB ($+3.7 \pm 2$, 2σ, Tomascak et al., 2008) and the range of CIA in unweathered basalts.

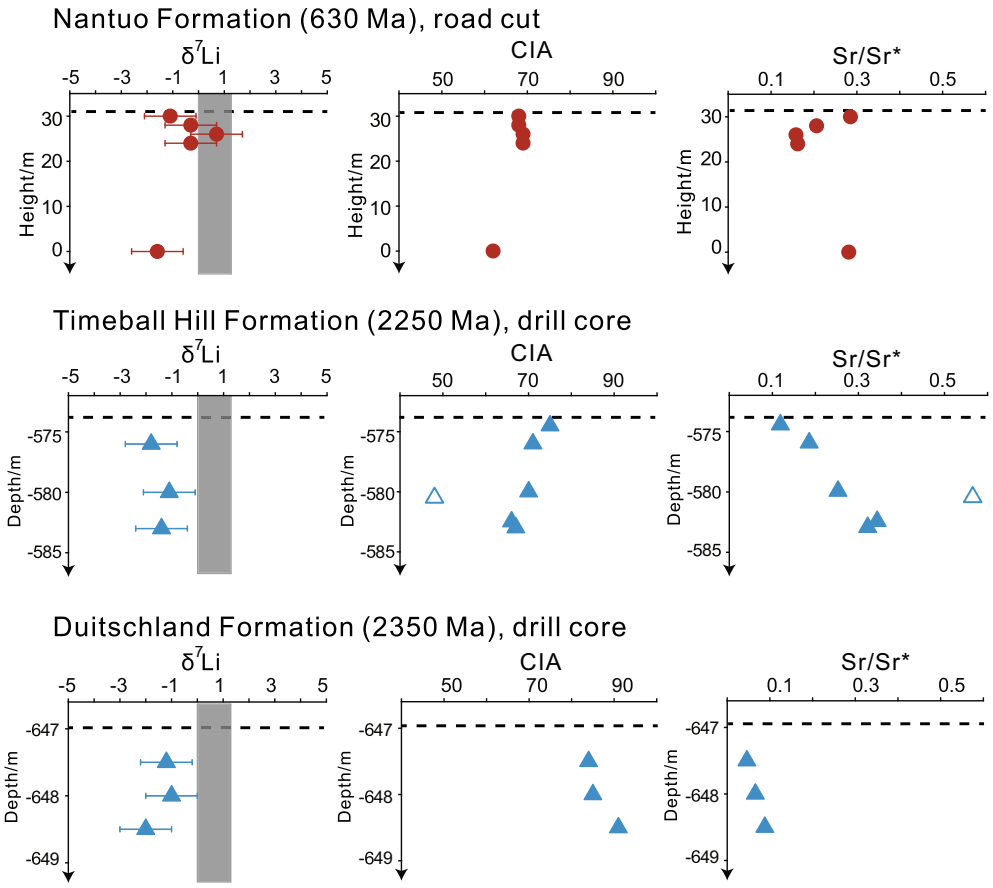

Fig. 2. δ^7Li, CIA and Sr/Sr* in profiles (road cut and drill core) through the top contact of three different diamictites (Sr/Sr* = Sr/(Ce*Nd)$^{0.5}$ where Sr, Ce, and Nd in the formula are normalized to average UCC of Rudnick and Gao, 2003). *Top:* Nantuo Formation, road cut. *Middle*: Timeball Hill Formation, drill core. *Bottom:* Duitschland Formation, drill core. Uncertainty on δ^7Li represents long term precision of ±1‰ (2σ). Two sigma uncertainty for CIA (±0.8%, 2σ) and Sr/Sr* (±2.4%, 2σ) are equal to or smaller than the size of the symbols. Horizontal line at the top of Nantuo Formation profile marks the contact with the overlying cap dolomite, horizontal line at the top of Timeball Hill and Duitschland Formation panels marks the contact with overlying lithologies, which are mudrocks and finely laminated shales, respectively. Vertical gray band in each profile marks average δ^7Li of the UCC (+0.6 ± 0.6, 2σ, Sauzéat et al., 2015). For the Timeball Hill Formation profile, δ^7Li of three samples were analyzed, whereas CIA and Sr/Sr* values of three additional samples and are plotted and given in Table 1. One carbonate-bearing sample is shown as an open triangle; otherwise, symbols are as in Fig. 1.

physical weathering during erosion, transport and deposition of muddy glacial sediments, and Canil and Lacourse (2011) demonstrated that glacial tills from the Canadian Cordillera provide a robust estimate for the bulk composition of the juvenile upper continental crust of British Columbia. Furthermore, lithified glacial tills (i.e., glacial diamictites) are recognized throughout much of the geologic record, going back to at least 2.9 Ga (Young et al., 1998), thus providing the opportunity to evaluate the secular evolution of the composition of the upper continental crust. Nevertheless, our recent study of the fine-grained matrix of glacial diamictites deposited from the Mesoarchean to the Paleozoic shows the surprising result that most of these samples possess a chemical weathering signature (Gaschnig et al., 2014). Their CIA values are generally greater than those of igneous rocks, and they show pervasive depletion in Sr relative to average upper continental crust (Gaschnig et al., 2014). Many samples, particularly those Neoproterozoic and younger, also show depletion in metals whose solubility is enhanced in their oxidized states, such as Mo and V, indicative of oxidative weathering (Gaschnig et al., 2014). Determining the origin of this weathering signature is important if one wishes to use the diamictite data to understand whether the UCC has an average composition impacted by weathering, or whether the nature of continental weathering has changed through time.

In this paper we use lithium and lead isotopes, in combination with previously published geochemical data, to evaluate the origin of the weathering signature in the glacial diamictites (i.e., is it pre-, syn-, or post-depositional in origin, or some combination thereof?). Finding that the signature is largely inherited from the source rocks, we use these data, along with data from other fine-grained terrigenous sediments to evaluate how chemical weathering of the upper continental crust might have changed through time.

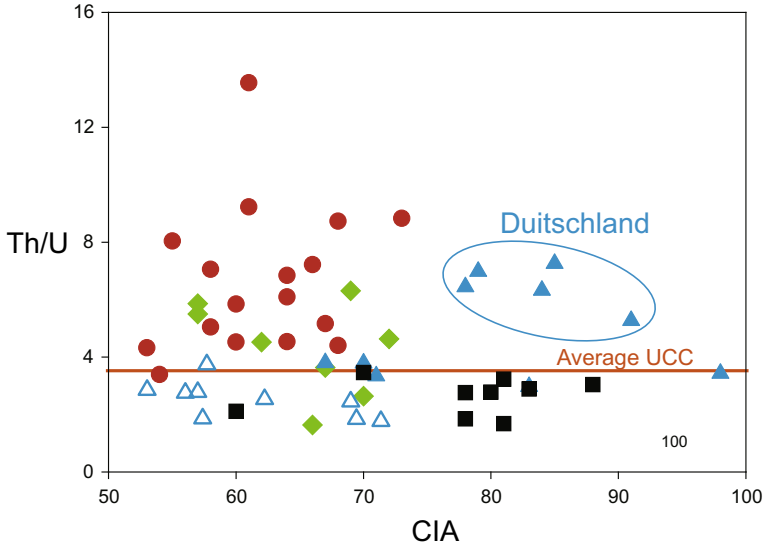

Fig. 3. CIA vs. Th/U for glacial diamictites. Nearly all Neoproterozoic and Paleozoic diamictites, along with a subset of Paleoproterozoic samples, have higher Th/U ratios than that of the average UCC (Rudnick and Gao, 2003), reflecting loss of U during oxidative weathering. Symbols as in Fig. 1.

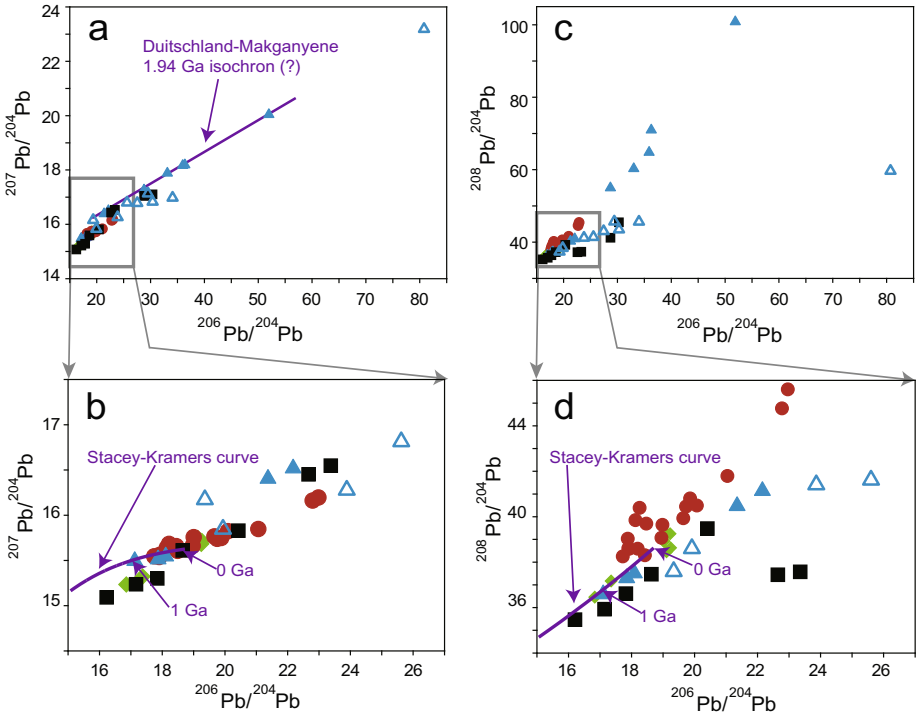

Fig. 4. Pb isotope plots. (b) and (d) are expanded views of the boxes in the lower left corners of (a) and (c), respectively. Two sigma standard error bars in the lower panels are approximately the size of the symbols. The Stacey and Kramers (1975) curve for terrestrial Pb evolution is shown. Many of the Paleoproterozoic South African samples have extremely radiogenic Pb isotopic compositions and are collinear, forming an apparent isochron of 1.94 Ga. See text for discussion. Symbols as in Fig. 1.

2. THE USE OF LITHIUM AND LEAD ISOTOPES TO TRACE CHEMICAL WEATHERING

Both Li and Pb isotopes can be used to document chemical changes associated with subaerial weathering, the former through mass-dependent fractionation associated with the development of secondary minerals, and the latter through changes in U/Pb and Th/U ratios created by uranium leaching under oxidizing conditions. We review the application of each isotope system, in turn.

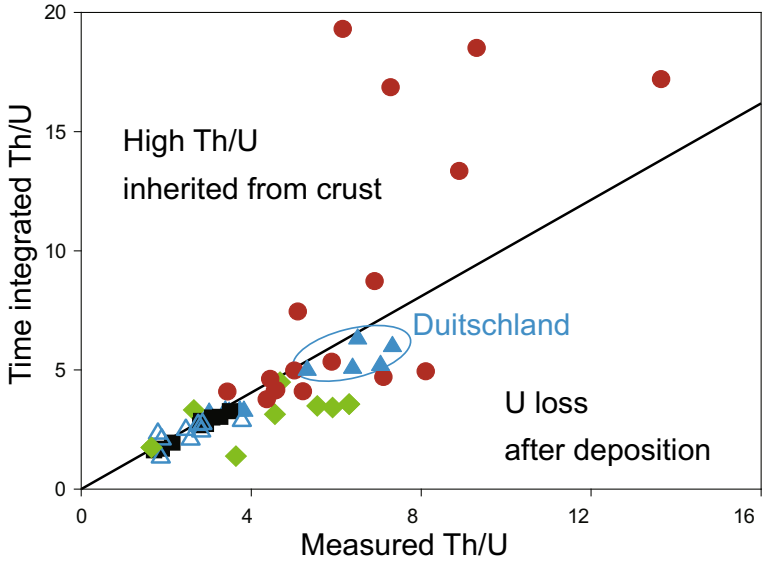

Fig. 5. Measured or instantaneous Th/U ratios vs. the time-integrated Th/U ratios calculated from Pb isotope compositions. The latter were calculated by assuming that the samples began on the Stacey and Kramers (1975) model curve at an age point equivalent to their depositional age and solving for the Th/U ratio required for the samples to reach their measured present-day compositions. The inclined black line in the plot is the 1:1 line. Samples with a higher time-integrated Th/U ratio than the measured values likely inherited their high Th/U ratio from the pre-existing crust that the ice sheets eroded, while those with a lower time-integrated Th/U ratio than their instantaneous values likely experienced post-depositional loss of U. Symbols as in Fig. 1.

2.1. Lithium

Lithium has several advantages as a tracer of chemical weathering. Lithium is soluble and has two stable isotopes, ^{6}Li and ^{7}Li, with ~17% mass difference, so lithium isotopes have significant potential for mass dependent fractionation. Lithium is not a critical component of biological or atmospheric cycles, and lithium is not sensitive to redox reactions because it has only one redox state (+1). Numerous studies have shown that lithium isotopes fractionate significantly during subaerial chemical weathering (Huh et al., 2001; Pistiner and Henderson, 2003; Rudnick et al., 2004; Kisakürek et al., 2005; Vigier et al., 2009; Pogge von Strandmann et al., 2006, 2010; Millot et al., 2010; Wimpenny et al., 2010a; Rad et al., 2013; Liu et al., 2013, 2015; Dellinger et al., 2014, 2015; Pogge von Strandmann and Henderson, 2015; Wang et al., 2015), with regoliths becoming isotopically light and waters heavy as Li partitions between octahedral coordination in secondary minerals and tetrahedral coordination in water. Different types of secondary minerals formed during chemical weathering cause different magnitudes of Li isotope fractionation (Pistiner and Henderson, 2003; Teng et al., 2004; Rudnick et al., 2004; Huh et al., 2004; Kisakürek et al., 2004; Williams and Hervig, 2005; Wimpenny et al., 2010b). Residues of intense crustal weathering, such as saprolites, laterites, and bauxites, can develop very low δ^{7}Li down to −20 (Rudnick et al., 2004; Kisakürek et al., 2004; Liu et al., 2013), and ocean water and river water have correspondingly high δ^{7}Li (e.g., ocean water: δ^{7}Li = +31, river water δ^{7}Li = 5–44; Chan and Edmond, 1988; You and Chan, 1996; Huh et al., 1998; Millot et al., 2004; Kisakürek et al., 2005; Pogge von Strandmann et al., 2006, 2010; Lemarchand et al., 2010; Liu et al., 2015). The continental crust is characterized by lower δ^{7}Li values (upper continental crust: $+0.6 \pm 0.6$, 2σ, Sauzéat et al., 2015; bulk continental crust: +1.2, Teng et al., 2008, and +1.7, Teng et al., 2009) than mantle-derived MORB ($+3.7 \pm 2$, 2σ, Chan et al., 1992; Moriguti and Nakamura, 1998; Elliott et al., 2006; Tomascak et al., 2008). Because of these features, Li isotopes have been proposed to provide a means by which to estimate the mass loss from the continents due to chemical weathering (Liu and Rudnick, 2011) and track continental weathering through time using the δ^{7}Li of seawater recorded in the tests of foraminifera (Hathorne and James, 2006; Misra and Froelich, 2012; Pogge von Strandmann et al., 2013; Li and West, 2014; Wanner et al., 2014; Vigier and Goddéris, 2015).

Studies of the behavior of Li isotopes in subaerial weathering profiles set the stage for the use of Li to investigate the origin of the weathering signature seen in the glacial diamictites. As a result of chemical weathering, δ^{7}Li decreases towards the surface as weathering intensity increases. Rudnick et al. (2004) found that saprolites developed on igneous rocks in South Carolina are consistently isotopically lighter than the unweathered igneous rocks, with δ^{7}Li ranging down to −20, one of the lightest isotopic compositions ever recorded for both bulk rock material and individual minerals. However, Li isotope behavior in weathering profiles can be complicated by additional factors such as diffusion, or deposition of marine aerosols or eolian dust. For example, Teng et al. (2010) suggested that the Li isotopic irregularities observed by Rudnick et al. (2004) in the saprolite profile were the result of diffusion processes. The equilibrium isotope fractionation produced by weathering lowered δ^{7}Li, and subsequent kinetic isotope

Table 1
Li and Pb isotopic compositions and other geochemical parameters of glacial diamictites.

Sample ID	Age (Ma)	Location	δ^7Li	[Li] ppm	Li/Al[1]	CIA	Sr/Sr*	^{206}Pb/^{204}Pb/ 2σ	^{207}Pb/^{204}Pb/ 2σ	^{208}Pb/^{204}Pb/ 2σ	Pb	Th	U	Th/U	Th/U*	Height (m)
Cenozoic Glaciomarine Sediments																
248150-2BBSB 1/6	0.015	Greenland	1.8	43.4	2.71	47	0.66									
GRL-8047	0.015	Hudson Straight		35.5			0.79									
GRL-8049	0.015	Hudson Straight		36.5			0.77									
Paleozoic																
West Dwyka Group		South Africa														
GKP01-122	300		2.3	40.6	3.27	62	0.44	17.353/8	15.331/7	37.184/17	16.34	7.32	1.61	4.54	3.20	−122
GKP01-127	300			53.2	4.10	66	0.18	19.239/10	15.723/8	38.644/19	31.71	11.25	6.92	1.63	1.81	−127
GKP01-129	300			22.5	3.92	69	0.37	16.832/16	15.243/16	36.474/38	11.50	3.90	0.62	6.29	3.62	−129
GKP01-140	300		2.2	19.3	3.01	67	0.54	19.110/19	15.755/15	38.473/41	8.64	4.09	1.13	3.62	1.45	−140
East Dwyka Group		South Africa														
13RMG012	300		−1.8	35.7	2.39	57	0.38	19.017/4	15.713/3	38.933/8	28.40	18.90	3.44	5.50	3.55	
13RMG016	300		−1.5	32.6	2.23	55	0.40									
13RMG017	300		0.1			55										
13RMG018	300		−0.3	31.7	2.09	57	0.40	19.023/6	15.700/5	38.931/11	29.90	20.40	3.48	5.86	3.48	
Mandiyuti Group		Bolivia														
BP-080307-8	300		2.9	29.8	2.96	70	0.21	19.222/3	15.692/3	39.266/6	14.78	10.38	3.94	2.63	3.38	
BP-080307-8 replicate			1.9													
BP-080307-8 average			2.4													
Machareti Group		Bolivia														
Machareti-4	330		3.6	84.8	5.34	75	0.30									
Machareti-4 replicate			3.4													
Machareti-4 redissolution			2.8													
Machareti-4 average			3.3													
Machareti-6	330		1.2	68.2	4.19	72	0.37	19.086/2	15.685/2	39.276/5	15.30	16.30	3.51	4.63	4.54	
Machareti-6 replicate			2.2													
Machareti-6 redissolution			1.7													
Machareti-6 average			1.7													
Pakhuis Formation		South Africa														
MBR299335	450		2.0	36.4	3.17	71	0.23									
Neoproterozoic																
Gaskiers Formation		Newfoundland, Canada														
K13-NFL-GF-A	580		1.7	42.7	2.76	58	0.49									
K13-NFL-GF-A replicate			2.0													
K13-NFL-GF-A average			1.9													
K13-NFL-GF-B	580		0.4	27.8	1.99	58	0.57									
K13-NFL-GF-C	580		−2.0	30.3	1.92	55	0.74									
K13-NFL-GF-D	580		−1.8	35.7	2.33	57	0.43									
Nantuo Formation		South China														
NT01	630		0.1	24.7	4.32	67	0.30									
NT02	630		−0.7	31.4	2.11	66	0.19	17.925/2	15.567/1	38.608/4	17.00	10.30	1.42	7.22	16.9	

(*continued on next page*)

Table 1 (*continued*)

Sample ID	Age (Ma)	Location	δ^7Li	[Li] ppm	Li/Al[1]	CIA	Sr/Sr*	^{206}Pb/^{204}Pb/2σ	^{207}Pb/^{204}Pb/2σ	^{208}Pb/^{204}Pb/2σ	Pb	Th	U	Th/U	Th/U*	Height (m)
NT03	630		−2.7	28.0	1.91	64	0.21									
NT03 replicate			−2.4													
NT03 average			−2.6													
NT04	630		−2.0	36.8	2.53	65	0.29									
NT05	630		−4.6	55.1	3.38	60	0.30									
NT05 replicate			−3.2													
NT05 average			−3.9													
NT05-2A	630		−1.1	37.1	2.69	68	0.29	17.725/2	15.557/2	38.273/7	21.00	11.00	1.26	8.73	140	30
NT05-2B	630		−0.3	39.5	2.99	68	0.21									28
NT05-2C	630		0.7	39.1	2.91	69	0.16									26
NT05-2D	630		−0.3	34.7	2.50	69	0.16									24
NT06	630		−1.6	39.4	2.70	62	0.28									0
NT07	630		2.1	34.6	2.45	63	0.28									
NT08	630		−2.0	34.8	2.38	64	0.19	17.895/2	15.565/2	38.605/5	16.30	9.76	1.60	6.09	19.3	
NT08 SAV*								17.888/2	15.563/2	38.612/4						
NT08 average								17.891/2	15.564/2	38.608/4						
Gucheng Formation		South China														
GCH-05	700		−2.4	36.0	2.40	73	0.08	17.882/3	15.546/2	39.042/6	13.90	10.50	1.19	8.83	13.4	
Konnarock Formation		Virginia, USA														
12RMG009	700			28.6	1.90	60	0.14	18.949/14	15.669/12	39.081/27	28.79	15.93	3.51	4.54	4.18	
12RMG012	700		0.6	26.0	1.83	58	0.15	19.727/2	15.742/1	40.447/3	15.80	22.90	3.26	7.05	4.75	
12RMG013C	700		0.7	24.9	1.81	54	0.19	19.857/3	15.751/3	40.805/7	10.50	21.10	2.62	8.04	4.99	
12RMG013C SAV*								19.866/3	15.750/2	40.832/5						
12RMG013C average								19.861/3	15.751/2	40.818/6						
Neoproterozoic																
Pocatello Formation		Idaho, USA														
12RMG016	700		−1.8	50.2	4.25	71	0.22									
12RMG016 replicate			−1.4													
12RMG016 average			−1.6													
12RMG017	700		0.5	18.7	1.47	68	0.07	22.771/5	16.165/3	44.764/9	6.24	18.30	4.16	4.40	4.67	
12RMG017 replicate			0.3													
12RMG017 average			0.4													
12RMG022	700		1.7	41.2	2.79	67	0.11	20.074/2	15.831/1	40.505/4	31.60	21.30	4.12	5.16	4.15	
12RMG022 replicate			2.0													
12RMG022 average			1.9													
Blauberker Formation		Namibia														
13RMG021	700		−0.7													
13RMG022	700		−1.7	21.7	2.20	53	0.35	18.422/1	15.661/1	38.301/2	14.00	7.95	1.84	4.32	3.82	
13RMG022 replicate			−1.2													
13RMG022 average			−1.5													
13RMG025	700		−1.1	19.0	1.86	62	0.16									
Numees Formation		Namibia														
13RMG034	700		−3.9	29.5	2.61	58	0.29	18.196/2	15.690/2	38.601/4	41.80	15.50	3.08	5.04	7.49	
13RMG034 replicate			−3.0													
13RMG034 average			−3.5													

13RMG039	700		−2.2	32.4	2.45	59	0.25								
13RMG040	700		1.3	23.4	1.61	61	0.15	18.255/2	15.655/2	40.391/4	26.70	30.10	2.22	13.5	17.2
13RMG040 redissolution (Pb analysis)								18.253/2	15.653/2	40.386/4					
13RMG040 average								18.254/2	15.654/2	40.389/4					
13RMG041	700		−0.2	20.5	1.44	61	0.21	18.127/2	15.652/2	39.874/4	29.10	28.90	3.13	9.23	18.5
13RMG046	700		2.1	30.3	3.59	64	2.12								
Chuos Formation		Namibia													
13RMG053	700		2.1	43.1	5.55	60	0.52	18.977/3	15.760/2	39.643/6	11.70	7.48	1.28	5.84	5.39
13RMG054	700		2.5	37.7	4.78	56	0.51								
Kaigas Formation		Namibia													
13RMG030	700		−1.4	41.0	2.67	54	0.37	19.641/3	15.773/3	39.946/6	35.60	27.60	8.15	3.39	4.14
Paleoproterozoic															
Gowganda Formation		Ontario, Canada													
12RMG045 (varvite)	2300		5.6	19.5	1.22	60	0.28								
12RMG053	2300		0.7	17.5	1.18	59	0.65								
12RMG053 redissolution			1.1												
12RMG053 average			0.9												
12RMG055	2300			11.0	0.81	56	0.35	23.862/31	16.286/22	41.426/54	7.85	11.81	4.33	2.73	2.76
12RMG057	2300			15.43	1.01	53	0.41	29.468/30	17.153/18	45.896/50	10.27	13.70	4.84	2.83	2.79
12RMG066	2300		2.7	13.7	1.09	49	1.47								
12RMG067	2300			21.6	1.73	58	0.50	19.914/2	15.855/2	38.613/4	6.58	3.49	0.94	3.74	2.92
Bruce Formation		Ontario, Canada													
12RMG042	2325		0.7	18.7	1.32	57	0.35	30.346/3	16.851/2	43.705/5	6.84	12.40	6.70	1.86	2.15
12RMG043	2325			33.6	1.93	62	0.33	34.046/4	16.999/2	45.853/6	6.42	20.10	7.95	2.53	2.14
Pecors Formation		Ontario													
12RMG048	2350			55.4	3.30	69	0.13	19.3366/8	16.181/9	37.607/18	47.17	11.89	4.87	2.44	2.55
Ramsay Lake Formation		Ontario, Canada													
12RMG037	2350			28.7	2.65	69	0.054	80.638/12	23.196/4	59.838/9	4.18	19.1	10.8	1.84	1.39
12RMG050	2350		2.9	62.0	3.92	71	0.22	25.599/3	16.821/2	41.634/4	6.58	4.53	2.57	1.77	2.39
12RMG050 replicate	2350		1.9												
12RMG050 average			2.4												
12RMG051	2350		2.6	70.0	5.44	68	0.19		.						
12RMG051 replicate	2350		2.3												
12RMG051 redissolution			2.5												
12RMG051 average			2.5												
Bottle creek formation		Wyoming, USA													
12RMG032	2350			10.6	0.808	57	0.83	27.499/4	16.801/2	43.231/6	6.38	7.10	2.54	2.78	2.48
12RMG033	2350		2.8	14.9	1.11	59	1.01								
12RMG033 replicate			4.2												
12RMG033 average			3.5												
Paleoproterozoic															
Makganyene Formation		South Africa													
GIF01-25	2350			17.8	2.54	92	0.28	19.884/2	16.256/2	38.941/5	21.40	9.72	2.93	3.32	3.16	25
GIF01-27.5	2350		0.6	14.6	2.44	98	0.33	21.351/3	16.412/2	40.492/5	12.70	7.93	2.31	3.43	3.28	27.5
GIF01-27.5 replicate			1.7												
GIF01-27.5 average			1.2												

(*continued on next page*)

Table 1 (*continued*)

Sample ID	Age (Ma)	Location	δ^7Li	[Li] ppm	Li/Al[1]	CIA	Sr/Sr*	^{206}Pb/^{204}Pb/ 2σ	^{207}Pb/^{204}Pb/ 2σ	^{208}Pb/^{204}Pb/ 2σ	Pb	Th	U	Th/U	Th/U*	Height (m)
GIF01-41.2	2350		0.2	21.3	2.42	86	0.13									41.2
GIF01-41.2 redissolution			0.8													
GIF01-41.2 average			0.5													
GIF01-44	2350			19.9	2.20	83	0.12	22.151/2	16.522/1	41.141/3	16.90	12.90	4.33	2.97	3.25	44
Timeball Hill Formation		South Africa														
EBAI574.5	2250			22.0	1.12	75	0.12									−574.5
EBAI576	2250		−1.8	35.4	2.22	71	0.19	17.101/2	15.504/2	36.606/4	97.20	13.60	4.08	3.34	3.34	−576
EBAI580	2250		−1.1	38.5	2.42	70	0.25	18.09/18	15.55/16	37.51/40	27.00	13.60	3.60	3.79	3.33	−580
EBAI580.5	2250			15.9	1.44	48	0.57									−580.5
EBAI582.5	2250			34.2	2.27	66	0.34									−582.5
EBAI583	2250		−1.4	38.5	2.49	67	0.32	17.851/2	15.526/2	37.324/4	30.70	14.40	3.90	3.69	3.34	−583
Duitschland Formation		South Africa														
EBAI1191	2350		2.3	43.3	1.76	78	0.1	51.889/17	20.049/7	100.846/35	6.25	25.20	3.91	6.44	6.35	−1191
EBAI1192	2350		0.3	60.7	2.61	79	0.05	28.747/4	17.280/2	55.138/7	20.60	37.50	5.38	6.98	5.24	−1192
DP22647.5	2350		−1.2	61.7	5.69	84	0.07	35.910/7	18.180/4	64.950/12	3.90	14.70	2.33	6.32	5.12	−647.5
DP22648	2350		−1.0	67.5	6.14	85	0.09	36.303/9	18.203/4	71.078/16	3.60	14.70	2.02	7.26	6.03	−648
DP22648.5	2350		−2.0	75.0	9.93	91	0.34	33.070/16	17.901/9	60.457/29	3.74	8.11	1.54	5.27	5.04	−648.5
Mesoarchean																
Mozaan Group		South Africa														
13RMG005	2900		−1.6	18.3	2.04	71	0.45									
13RMG006	2900		−2.3	20.0	2.28	72	0.12									
13RMG007	2900		−3.3	24.1	2.70	88	0.29	18.627/3	15.614/2	37.471/6	8.93	3.65	1.20	3.04	3.06	
13RMG008	2900		−2.8	21.1	2.33	74	0.64									
13RMG009	2900		−3.7	20.5	2.16	72	1.12									
13RMG009 replicate			−3.1													
13RMG009 average			−3.4													
13RMG010	2900		−2.3	19.5	2.29	70	1.83	20.405/2	15.837/2	39.494/5	3.55	3.42	0.99	3.46	3.33	
13RMG011	2900			19.8	2.53	81	0.30	16.203/1	15.097/1	35.475/3	9.86	3.06	0.95	3.23	3.09	
Afrikander Formation		South Africa														
13RMG001	2900		−1.8	21.1	2.49	80	0.1	17.818/3	15.306/2	36.617/6	2.97	1.36	0.49	2.78	2.92	
13RMG003	2900			19.9	2.39	83	1.93	17.141/3	15.245/2	35.944/6	4.35	1.55	0.54	2.89	2.79	
Promise Formation		South Africa														
BABI-4031	2900		−3.0	70.1	4.53	78	0.24	30.325/5	17.126/3	45.689/8	6.52	5.22	1.89	2.76	2.74	
BABI-4031 replicate			−2.0													
BABI-4031 average			−2.5													
BABI-4042	2900			5.57	0.776	60	0.10	28.764/5	17.068/3	41.437/8	1.86	1.30	0.62	2.11	2.01	
Coronation Formation		South Africa														
BABI-3171	2900		−0.2	32.5	2.15	78	0.34	22.644/3	16.460/2	37.459/5	18.6	7.39	3.99	1.85	1.76	
BABI-3171 replicate			−0.4													
BABI-3171 average			−0.3													
BABI-3216	2900			34.0	2.17	81	0.27	23.354/4	16.556/3	37.589/7	18.8	7.09	4.22	1.68	1.69	

Notes: 1. Li/Al is Li concentration in ppm divided by Al_2O_3 in weight percent. Two-sigma error for δ^7Li is <1. Sr/Sr* (=Sr/(Ce*Nd)$^{0.5}$) is the relative Sr concentration. Th/U indicates "measured Th/U", Th/U* indicates "time integrated Th/U". "SAV*" indicates Pb isotope analysis from powder aliquot dissolved on hot plate in Savillex beaker rather than bomb. Redissolution means independent sample dissolution and column chemistry. Replicate means independent column chemistry. CIA, Al_2O_3 and Sr/Sr* values are from Gaschnig et al., 2014.

fractionation during diffusion further decreased the δ^7Li values. Studies of soil profiles developed on Hawaiian basalt attributed the variable but generally heavy lithium to the uptake of aerosol lithium derived from seawater (Huh et al., 2004). Following Huh et al. (2004), Pogge von Strandmann et al. (2012) also observed highly variable δ^7Li through a basaltic soil profile from a well-characterized Histic Andosol in south-west Iceland. Diffusion processes were determined not to be significant and most of the soils had lower δ^7Li than the unweathered basalt and associated pore waters, though a few samples had very high δ^7Li, which was attributed to the presence of sea-water aerosols. δ^7Li through a profile of bauxites developed on the Miocene Columbia River Basalts was observed to decrease systematically towards the surface, while Li concentrations increase systematically towards the surface (Liu et al., 2013). This anti-correlation between δ^7Li and [Li] was ascribed to addition of eolian dust to the top of the section. Despite these complications in the details of Li isotope behavior, there is a clear overall tendency for δ^7Li values to become lower in weathered continental material and for most profiles through weathering horizons to show systematic changes in δ^7Li with depth. Lithium isotopes can thus be used to evaluate post-depositional weathering of the tillites by looking at isotopic profiles through the units.

2.2. Lead

Lead has four stable isotopes (204, 206, 207, and 208). Two of these (206 and 207) are produced by the radioactive decay of ^{238}U and ^{235}U, respectively, and ^{208}Pb is produced by the decay of ^{232}Th. The ratios of ^{206}Pb, ^{207}Pb, and ^{208}Pb to ^{204}Pb in geologic material measured today are governed by a combination of age and time-integrated U/Pb, Th/Pb, and Th/U ratios. Of interest here is Th/U, which does not vary significantly during igneous differentiation but is affected by oxidative weathering, which mobilizes U in its soluble +6 oxidation state, leading to U loss and an increase in the Th/U or kappa value (^{232}Th/^{238}U). Adopting models for the isotopic evolution of terrestrial Pb (e.g., Stacey and Kramers, 1975), it is possible to use the Pb isotopic composition of geologic materials to determine their *time-integrated* kappa value, and by comparing this to measured present day Th/U (or *instantaneous* kappa), the timing of Th/U increase due to uranium leaching can be inferred. This approach has been applied to sedimentary rocks to determine whether their kappa values were disturbed after deposition due to fluid flow, metamorphism, or *in situ* weathering, or if kappa was affected by uranium removal during deposition (e.g., Krogstad et al., 2004; Pollack et al., 2009).

Here we report Li and Pb isotopic compositions of glacial diamictites spanning ages from the Archean to the Cenozoic. Combined with previously published major and trace element data (Gaschnig et al., 2014), we use these new isotopic data to evaluate the origin of the weathering signature recorded in these deposits. For glacial diamictites that are geographically dispersed (e.g., those from the Paleoproterozoic, Neoproterozoic), the δ^7Li signature of these deposits can be used to evaluate how the weathering signature in the upper continental crust may have changed through time.

3. SAMPLES

The glacial diamictites studied here formed from soils and rocks that were pulverized by continental ice sheets as they moved across broad swaths of the Earth's surface. They are essentially glacial tills that have been lithified by subsequent burial and consist of angular to rounded clasts of variable sizes in a fine-grained matrix. The matrix comprises a large percentage of the rock and is usually dark gray to greenish black in color. Evidence of glacial origin includes faceted and striated clasts of heterogeneous composition and the presence of dropstones in otherwise finely-laminated intervals. The glacial diamictites were deposited primarily in shallow marine settings, though a few were deposited above sea level (Appendix Table A1).

Glacial deposits occur in five broad geological periods: the Mesoarchean (ca. 2900 Ma; Young et al., 1998), Paleoproterozoic (2400–2200 Ma; Crowell, 1999; Bekker et al., 2001; Kopp et al., 2005; Melezhik et al., 2013), Neoproterozoic (750–550 Ma; Hoffman and Li, 2009), Paleozoic (a short glacial event at 450 Ma and a longer one at 330–300 Ma; Crowell, 1978; Visser, 1982; Caputo and Crowell, 1985; Hambrey, 1985) and Cenozoic (2.58–0.01 Ma; Pillans and Gibbard, 2012). The glacial diamictites investigated here come from all five of these periods, over five geographic regions: southern Africa, North America, southern China, South America and Greenland. The individual stratigraphic units are listed in Table 1, and their present geographic distribution is shown in Appendix Fig. A1.

In total, ninety-one glacial diamictites were investigated in this paper. Most of the samples were taken from outcrops, except for the Mesoarchean Coronation and Promise Formations, Paleoproterozoic Transvaal Supergroup, Ordovician Pakhuis Formation and some of the Paleozoic Dwyka Group samples, which were obtained from drill cores. All of the samples investigated here, save the modern glaciomarine sediments, were previously described, and major and selected trace elements are reported in Gaschnig et al. (2014).

4. ANALYTICAL METHODS

The diamictites were crushed to gravel-size fragments, after which the clasts larger than ~5 mm were separated from the matrix by hand. The matrix materials of each sample were then ground to fine powders in a ceramic swing mill.

Li, Pb, Th, and U concentrations were analyzed together with other trace elements on a Thermo-Finnigan Element 2 high resolution-ICP-MS in the Department of Geology at the University of Maryland. Details for the analyses are reported in Gaschnig et al. (2014). Samples were analyzed along with USGS whole-rock reference materials AGV-2, BHVO-1, GSP-1, and W-2 prepared at the same time as the samples. A constant amount of indium spike was added to each sample and used for drift correction. Elemental concentrations in samples were determined from calibration

curves constructed from the four USGS standards (AGV-2, BHVO-1, GSP-1, and W-2). Overall precision and accuracy were evaluated by repeat analysis of separately dissolved AGV-2 aliquots treated as unknowns, which yielded average concentrations of 11.5 ± 0.3, 15.9 ± 0.4, 6.62 ± 0.18, and 2.07 ± 0.05 ppm ($n = 7$) for Li, Pb, Th, and U, respectively, which fall within the range of published values reported in the GeoReM database (Jochum et al., 2005). Samples from the Konnarock, Nantuo, and Gucheng Formations were analyzed on an Agilent 7700× quadrupole ICP-MS in the State Key Laboratory for Geological Processes and Mineral Resources at the China University of Geoscience in Wuhan, China, broadly following the methods of Hu and Gao (2008). Calibration was conducted using multi-element standard solutions as a basis and adjusting this calibration after analysis of dissolved whole-rock standards (AGV-2, BHVO-2, BCR-2, RGM-1, GSR-5, GSS-8, and SCO-1) to best fit the published values for these standards.

In order to evaluate the effectiveness of our method of separating clasts and its potential influence on the whole rock composition, we made multiple powder aliquots from two samples of the Konnarock Formation. One powder aliquot from each sample was prepared from chips that had been handpicked to exclude small clasts and another aliquot was prepared from chips that were selected at random and not handpicked. The difference in major and trace element concentrations was $\leqslant 5\%$ for nearly all elements for one picked/unpicked pair and $\leqslant 10\%$ for the other pair. These data are reported in the Appendix Table A2.

Details of sample dissolution and column chemistry procedures for Li isotope analyses are reported in Rudnick et al. (2004) and instrumental analysis is described by Teng et al. (2004). Briefly, rock powders were dissolved in 16 mL Teflon, screw-cap beakers with a combination of concentrated HF and HNO_3, followed by HNO_3 and HCl addition to the dried residue. Perchloric acid was used, where needed, to dissolve samples containing organic carbon. Lithium analyses were conducted on a Nu Plasma MC–ICP-MS using the L-SVEC standard-bracketing method at the University of Maryland. Lithium isotopic compositions were normalized to that of L-SVEC and reported as δ^7Li. Two pure Li solutions, UMD-1 and IRMM-016, were analyzed during the course of each analytical session to monitor instrument performance and evaluate long-term external precision (estimated as <1.0 (2σ) based on duplicate analyses these Li solutions (Appendix Table A3). For example, IRMM-016 gives $\delta^7\text{Li} = +0.3 \pm 0.8$ (2σ, $n = 45$) and the in-house standard, UMD-1, gives $\delta^7\text{Li} = +55.1 \pm 0.8$ (2σ, $n = 48$) during the course of this study (July 2013 to July 2014). In addition, data for international rock standards (BHVO-1, BCR-2, G-2, AGV-1, GSP-1 and MAG-1) were measured during the course of this study and are presented in Appendix Table A4. Our values fall within the range for previously published results, where available; to our knowledge, our values for MAG-1 (-0.1) and GSP-1 (-3.5) are the first Li isotope data for these reference materials.

Pb isotopic analyses were performed on ~0.1 g splits of powder dissolved with 3 mL of HF and 1 mL of HNO_3 for a minimum of four days in sealed Parr bombs at ~180 °C in an oven. After drying down, samples were converted to chlorides with HCl, dried again, and then dissolved in 0.5 M HBr. A few samples were also dissolved on the hot plate in Savillex beakers for comparison to bomb-dissolved aliquots to see if bulk Pb isotope compositions were strongly influenced by refractory phases such as zircon. Three USGS reference materials were also dissolved in this manner. Solutions were loaded onto columns with BioRad AG-1X8 anion resins. Matrix elements were washed out with 0.5 M HBr and Pb was eluted with 8 M HCl. This column procedure was conducted twice in order to assure the purity of the Pb fraction.

Lead isotope analyses were conducted on a Nu Plasma MC-ICP-MS at the Department of Terrestrial Magnetism of the Carnegie Institution for Science in Washington, DC, and on a Nu Plasma MC-ICP-MS at the Department of Geology of the University of Maryland. Samples were doped with thallium solution to achieve a Pb/TI ratio of 5, and thallium was used to correct for mass fractionation. The NBS-981 Pb isotope standard (also doped with thallium) was analyzed repeatedly throughout each session, and samples were normalized to the standard using the values of Galer and Abouchami (1998). The average reproducibility (2σ) of NBS-981 for ^{206}Pb/^{204}Pb, ^{207}Pb/^{204}Pb, and ^{208}Pb/^{204}Pb was 0.04%, 0.06%, and 0.06%, respectively, at the Carnegie Institution, and 0.09%, 0.10%, and 0.11% at the University of Maryland. Values determined for USGS reference materials RGM-1 and BCR-2 (Appendix Table A5) overlap with the published range listed in GeoReM. Values determined for AGV-2 (Appendix Table A5) are less radiogenic than most published values but fall within the range for leachates reported by Weis et al. (2006). Since these reference materials were dissolved at low pressure on the hot plate, we are probably observing the same effects reported by Weis et al. (2006). Two samples, NT08 and 12RMG013C, were dissolved by both high pressure bomb and low pressure hot plate dissolution methods. In both cases, the ^{206}Pb/^{204}Pb ratios differ by amounts slightly outside of internal error, with the hot plate dissolved aliquot of NT08 being slightly less radiogenic and that of 12RMG013C being slightly more radiogenic than the Parr bomb dissolved complement. ^{208}Pb/^{204}Pb ratios are within internal error for NT08, but the hot plate dissolved aliquot has slightly more radiogenic ^{208}Pb/^{204}Pb for 12RMG013C. The most likely mineral to resist hot plate dissolution is zircon, but the relatively small differences between hot plate and bomb dissolved aliquots and the lack of consistently more radiogenic values seen in the bomb dissolved aliquots suggests that the contribution of zircon to the total Pb budget is not significant, at least for these two diamictites.

5. RESULTS

Lithium and Pb isotopic compositions of glacial diamictites are reported in Table 1, along with Li, Pb, Th, and U concentrations; CIA and Sr/Sr* values from Gaschnig et al. (2014) are also listed. Sr/Sr* (defined as $= \text{Sr}/(\text{Ce}^*\text{Nd})^{0.5}$, where Sr, Ce and Nd in the formula are normalized to

average UCC of Rudnick and Gao, 2003), is a measure of Sr enrichment or depletion relative to REE having a similar behavior during partial melting. Sr/Sr^* reflects the degree of weathering of a sample relative to an igneous composition, as Sr is one of the first elements to be removed from a crystalline rock via dissolution of disseminated carbonate (Jacobsen and Blum, 2000).

The δ^7Li values in the glacial diamictites range from −3.9 to +3.5, and are generally lower than those of mantle-derived basalts ($+3.7 \pm 2$, 2σ) (Tomascak et al., 2008). Li concentrations and Li/Al range from 14 to 85 ppm, and from 1.1 to 9.9, respectively. CIA and δ^7Li of the diamictites fall within the range of values observed in shale and loess (Bouman et al., 2004; Teng et al., 2004; Chan et al., 2006; Qiu et al., 2009, 2011; Appendix Table A6-1), and are distinctly higher and lower, respectively, than those of fresh mantle-derived basalts (Fig. 1). The relative concentration of Li in the diamictites, as reflected in the Li/Al ratio (Table 1), overlaps with the lower range of Li/Al in shales, though all Paleozoic and some Neoproterozoic (particularly the Chuos and some Nantuo Formation samples) and Paleoproterozoic diamictites (particularly the Ramsey Lake and the Duitschland 'DP' series samples) have high relative Li concentrations.

The δ^7Li, CIA and Sr/Sr^* in profiles through the top of diamictite units exposed in fresh road cuts and drill cores are plotted in Fig. 2; the δ^7Li values are mostly lower than that of upper continental crust ($+0.6 \pm 0.6$, 2σ) (Sauzéat et al., 2015), indicating a pervasive weathering signature throughout each of the profiles. Glacial diamictites within a single outcrop or from the same drill core have similar δ^7Li, Li/Al and CIA values but variable Sr/Sr^* values. For example, five samples from a road cut through the Nantuo Formation in South China show a range of δ^7Li from −1.6 to +0.7, [Li] from 35 to 40 ppm, Li/Al from 2.5 to 3.0 and CIA from 62 to 69, and all of these values lie with uncertainty of one another. By contrast, the Sr/Sr^* values, which range from 0.16 to 0.29, vary beyond uncertainty of one another. A drill core through seven meters of diamictite from the Timeball Hill Formation also shows overlapping δ^7Li and Li/Al values, with slightly increasing CIA and decreasing Sr/Sr^* towards the top of the unit. Another drill core through a meter thick section of diamictite from the Duitschland Formation has δ^7Li values that lie within uncertainty of one another but shows slightly decreasing CIA and Sr/Sr^* towards the top of the unit and variability in Li/Al values (Table 1).

δ^7Li values do not correlate with CIA (Fig. 1) or normalized Li concentration, but low values of δ^7Li can be accompanied by high CIA and low Sr/Sr^* values in some formations (Table 1). For example, the South African Mesoarchean glacial diamictites have the lowest average δ^7Li and highest average CIA, suggesting intense weathering, and show small variations in δ^7Li and Li/Al. By contrast, Paleoproterozoic diamictites show a significantly larger range of Li/Al (1.1–9.9) and δ^7Li (−2 to +3.5) than the Mesoarchean samples and their weathering indices correlate with geographic location: South African samples have lower average δ^7Li and higher average CIA, and therefore a stronger weathering signature than North American samples. The average δ^7Li values of Neoproterozoic and Paleozoic diamictites are -0.5 ± 3.4 (2σ) and $+1.0 \pm 3.6$ (2σ), respectively, indicating a weaker weathering signal in these samples. In general, the Archean and Paleoproterozoic samples have lower average δ^7Li and higher average CIA than post-Paleoproterozoic samples, suggesting more intense weathering earlier in Earth history.

The measured (instantaneous) Th/U of diamictite samples is compared to the average UCC Th/U (3.8, Rudnick and Gao, 2003) in Fig. 3. All of the Neoproterozoic, most of the Paleozoic and a subpopulation of the Paleoproterozoic samples have Th/U values higher than the average UCC. The Pb isotopic systematics of the samples is shown in Fig. 4 along with the terrestrial Pb growth curve of Stacey and Kramers (1975) (referred to as the SK curve below). Most of the Neoproterozoic samples plot in a cluster along the SK curve in $^{207}Pb/^{204}Pb$ vs. $^{206}Pb/^{204}Pb$ space, suggesting a time-integrated U/Pb ratio that is similar to that of the bulk Earth. Several Neoarchean samples have relatively nonradiogenic compositions suggesting a low time integrated U/Pb, which is consistent with their low measured U/Pb. Some of the Paleozoic samples from the western portion of the Dwyka Group contain similarly nonradiogenic Pb, suggesting a mainly Archean provenance, an interpretation consistent with high concentrations of first-row transition metals, and the Paleoproterozoic to Archean ages of the detrital zircons they contain (Gaschnig et al., 2014, 2015). Numerous Paleoproterozoic samples, mostly those from South Africa, have extremely radiogenic $^{207}Pb/^{204}Pb$ and $^{206}Pb/^{204}Pb$ ratios, requiring very high time-integrated U/Pb. Interestingly, all but one of the samples of the Paleoproterozoic Makganyene and Duitschland Formations fall along a linear array corresponding to a Pb–Pb date of 1.94 Ga. Using the reproducibility of the NBS-981 standard as the uncertainty on the data points yields a well constrained isochron age of 1.94 ± 0.03 with an MSWD of 0.39. The significance of this apparent isochron is discussed below. In $^{208}Pb/^{204}Pb$ vs. $^{206}Pb/^{204}Pb$ space, the SK model forms an essentially straight line, corresponding to a Th/U of 3.8. Assuming that each diamictite represents a mixture of crustal material that originally fell along the SK model, the time-integrated Th/U for each diamictite sample can be determined by measuring the slope of the line that connects its measured isotopic composition to the SK isotopic composition at the time of its deposition. A comparison of this time integrated Th/U to the measured Th/U for each sample is shown in Fig. 5. About half of the Neoproterozoic samples have time-integrated Th/U values significantly higher than their present day values, whereas a few Paleoproterozoic, Neoproterozoic, and Paleozoic samples have moderately lower time integrated values than their present day values.

6. DISCUSSION

6.1. Chemical and Li isotope evidence for the origin of the chemical weathering signature in glacial diamictites

The glacial diamictites exhibit pervasive chemical weathering signatures manifested by higher CIA values than

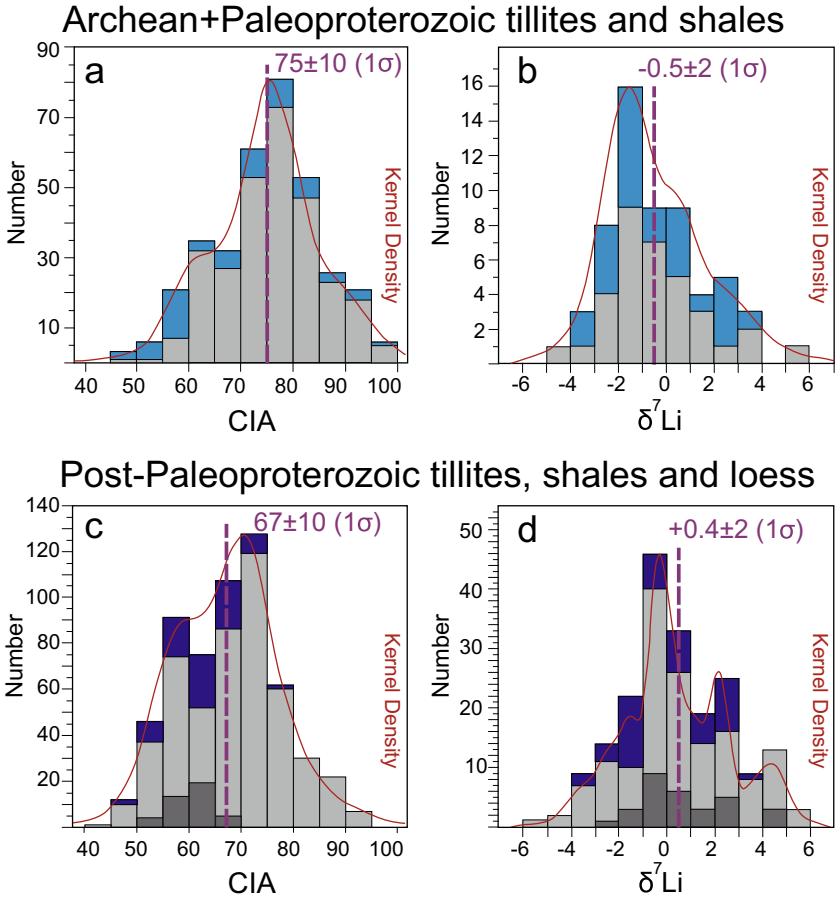

Fig. 6. Histograms of CIA and Li isotopic compositions (a and b, respectively) for Archean + Paleoproterozoic tillites (blue) and shales (gray; data compiled from the literature); (d) and (c) are histograms of Li isotopic compositions and CIA values for post-Paleoproterozoic sedimentary rocks (dark blue are glacial diamictites; gray bars are shales and dark gray bars are loesses; the latter two data sets were compiled from the literature). The curved red solid line in each diagram is the Kernel density plot of the data, which shows that the CIA and δ^7Li values of the post-Paleoproterozoic samples are skewed towards lower and higher values, respectively. The vertical dashed line in each diagram marks the average of all of the data in each histogram. The average CIA values of the post-Paleoproterozoic rocks are lower and the δ^7Li values are higher than corresponding data for the Archean + Paleoproterozoic rocks. Diamictite data are from Table 1. Archean shale data are provided in Appendix Table A6. Post-Paleoproterozoic sedimentary rock data, including loess, shales, clay, and pelite, are from the references listed in Appendix Table A6. (For interpretation of the references to colour in this figure legend, the reader is referred to the web version of this article.)

observed in igneous rocks and significant Sr depletion relative to average upper continental crust (Gaschnig et al., 2014). The Li isotopic data obtained in this study are consistent with a ubiquitous chemical weathering signature. The δ^7Li values are systematically lower than those of fresh MORB ($+3.7 \pm 2$, 2σ, Tomascak et al., 2008. Fig. 1), and overlap that of average upper continental crust, as sampled by shales, loess, and granites (Bouman et al., 2004; Teng et al., 2004; Chan et al., 2006; Manikyamba and Kerrich, 2006; Qiu et al., 2009, 2011; Sauzéat et al., 2015; Appendix Table A6-1). This isotopically light signature of upper continental crust has been attributed to the influence of chemical weathering (Teng et al., 2004; Sauzéat et al., 2015).

There are three possible origins of the weathering signature seen in diamictites: (1) in-situ weathering of the diamictite following deposition (post-depositional weathering), (2) chemical weathering that occurs during glacial erosion and sediment transport (syn-depositional weathering), and (3) inheritance of the weathering signature from the crustal material that is being eroded by the glaciers (pre-depositional weathering). These three possibilities are not mutually exclusive, as weathering may have occurred at more than one time and in more than one episode. We use the combined geochemical, lithium and lead isotope data presented here to evaluate each of these possibilities.

6.1.1. Subaerial post-depositional weathering

Nearly all of the diamictites studied here were deposited underwater (Appendix Table A1). These submarine deposits are generally conformably overlain by other sedimentary deposits, suggesting that there was little opportunity for subaerial post-depositional weathering to have occurred. Furthermore, if subaerial weathering had occurred and was severe enough, a paleosol would be developed at the upper boundary of the unit. No paleosols were observed in any of the glacial diamictites sampled in outcrop or in

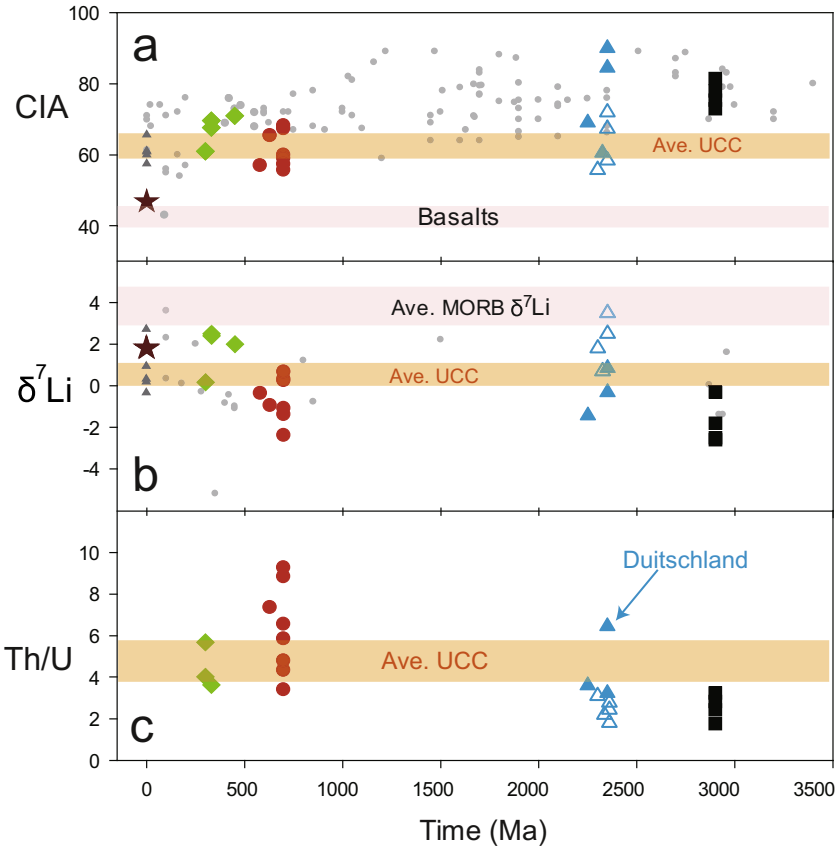

Fig. 7. CIA (upper), δ^7Li values (middle) and Th/U (lower) through time. For CIA, δ^7Li and Th/U, the diamictite data points are averages for the different stratigraphic units, and the shale data points are averages for different references (see Appendix Table A6-2 for tillite formation averages and shale reference average data). Most Archean and Paleoproterozoic glacial diamictites and shales have higher CIA and lower δ^7Li than those of most post-Paleoproterozoic sedimentary rocks (including glacial diamictites, loess, shales, clay, pelite). The pink box represents the δ^7Li range of fresh MORB (3.7 ± 2, 2σ, Tomascak et al., 2008), the range of CIA for basalts (40–45), and the yellow box represents the range in δ^7Li ($+0.6 \pm 0.6$, 2σ, Sauzéat et al., 2015), CIA (59–65, 2σ, Sauzéat et al., 2015) and Th/U of average UCC (3.8–5.8). Th/U values are from Table 1 in this study, otherwise, see caption to Fig. 6 and Appendix Table A6 for data sources. The Duitschland diamictites have unusually high Th/U ratios, indicating a provenance that experienced strong oxidative weathering, even though these diamictites were deposited before the Great Oxidation Event on the basis of their sulfur isotope signatures (see Gaschnig et al., 2014, for discussion of this). Shales of all periods are shown as gray circles, otherwise, symbols as in Fig. 1. (For interpretation of the references to colour in this figure legend, the reader is referred to the web version of this article.)

drill cores (see Gaschnig et al., 2014, and Appendix Fig. A2).

Post-depositional subaerial weathering can also be recognized through the development of a chemical weathering profile within the diamictites, with geochemical evidence of more intense weathering higher in the stratigraphic section (e.g., Nesbitt and Young, 1982; Rudnick et al., 2004; Gong et al., 2013). Profiles through three of the units were taken in order to examine chemical evidence for weathering: the Neoproterozoic Nantuo Formation, which was sampled at a decimeter-scale along a fresh road cut, and the Paleoproterozoic Timeball Hill and Duitschland Formations, which were each sampled in their entirety in drill cores. Two of these three profiles (i.e., Nantuo and Duitschland Formation) do not show any systematic changes in CIA, δ^7Li or Sr/Sr* that would be expected if incipient subaerial weathering had occurred (Fig. 2). By contrast, Timeball Hill shows changes with depth that are consistent with post-depositional chemical weathering: CIA increases, and Sr/Sr* decreases towards the surface. However, there is no significant change in δ^7Li through this section, suggesting that the Li signature of the Timeball Hill diamictite was mainly inherited from the provenance of the sediments, which was also weathered, given the δ^7Li values of -1.1 to -1.8, minimum CIA of 67 and maximum Sr/Sr* of 0.32.

In summary, post-depositional weathering appears to have played a minimal role in generating the low δ^7Li, Sr/Sr* and high CIA in the majority of deposits investigated here. Only the Paleoproterozoic Timeball Hill Formation shows possible evidence of post-depositional weathering, and even here this signature was superimposed upon sediments that carried a weathering signature at the time of their deposition.

6.1.2. Syn-depositional weathering

To what degree might syn-depositional weathering have imparted the weathering signature seen in the glacial diamictites? Chemical weathering rates correlate exponen-

tially with temperature (Walker et al., 1981; Retallack, 1990; White and Blum, 1995). The cold temperatures prevalent during glaciations should thus limit syn-depositional weathering. Absence of chemical weathering during glacial transport and deposition was documented by Nesbitt and Young (1996) who observed low CIA values and no appreciable amounts of secondary aluminous phases, such as clay minerals, in modern glacial sediments from Guys Bight Basin on Baffin Island. Moreover, the bulk chemical composition of the Guys Bight Basin sediments, after suffering extreme comminution in the glacial environment, differs little from that of the source rocks. Minimal syn-depositional weathering is further supported by the absence of a weathering signature (e.g., low CIA of 47, modest Sr depletion with $Sr/Sr^* = 0.66$ and $\delta^7Li = +1.8$) in modern glaciomarine sediments from the Hudson Straight and off the coast of Greenland that derive from Archean shields whose regolith had been removed during prior glacial epochs (Fig. 1 and Table 1). We thus conclude that syn-depositional weathering was likely minimal in the glacial diamictites we have studied.

6.1.3. Inheritance of the weathering signature from the provenance

Given the lack of evidence for significant post- and syn-depositional weathering in these deposits cited above, it would seem that the high CIA, low δ^7Li and low Sr/Sr^* observed in most of the glacial diamictites likely reflects an intrinsic characteristic of the UCC that was eroded by the glaciers. In all cases but two (the Paleoproterozoic Bottle Creek Formation in Wyoming and the modern glaciomarine sediments from the North Atlantic), the diamictites show evidence of significant weathering, suggesting that the glaciers were sampling weathered regolith that existed at the surface of the Earth at the time of glaciation.

One curiosity is the contrast between the modern glaciomarine sediments and the ancient deposits. The youngest glacial sediments analyzed here, which derive from the last glacial period of the Pleistocene glaciations, show minimal influence of weathering in their bulk compositions, suggesting that the glaciers traversed largely unweathered igneous and/or metamorphic rock. This likely reflects removal of any weathered regolith by preceding Cenozoic glacial events, with insufficient time for the regolith to be re-established between glacial periods. The pervasive weathering signature seen in all older diamictites, save the Wyoming samples, suggests that Milankovitch-driven glacial cycles occurring over short intervals of tens to 100's of thousands of years may be unique to the Cenozoic, and that the time intervals between possible multiple glacial periods in pre-Cenozoic ice ages were long enough to produce a significantly weathered regolith. Certainly, the presence of a strongly weathered signature in all of the Neoproterozoic "snowball Earth" glaciations, for example: the Kaigas (ca. 770–735 Ma), Sturtian (ca. 715–680 Ma) and Marinoan (ca. 660–635 Ma) episodes, which repeat over time intervals of ~30 million years (Frimmel et al., 1996; Allen et al., 2002; Lund et al., 2003; Zhou et al., 2004; Condon et al., 2005), as well as the Paleoproterozoic glacial events, suggest that the time interval was long enough, and that the weathering intensity was great enough to produce a deep regolith between glacial intervals.

6.2. Evidence from Pb isotopes

If chemical weathering occurs under oxidizing conditions, uranium may be lost to solution, which will increase the Th/U ratio in the weathered regolith. Nearly all of the Neoproterozoic and Paleozoic diamictites and the Paleoproterozoic Duitschland diamictites have measured Th/U ratios higher than the average UCC (Rudnick and Gao, 2003; $Th/U = 3.8$) and bulk silicate Earth (McDonough and Sun, 1995; $Th/U = 3.9$) (Fig. 3), which is consistent with other studies that have found high ($\geqslant 4.0$) Th/U ratios in sedimentary rocks postdating the Paleoproterozoic Great Oxidation Event (e.g., McLennan and Taylor, 1980), and a parallel decrease in the Th/U in mantle basalts (e.g., Collerson and Kamber, 1999), attributable to the preferential loss of U from the continents during oxidative weathering and its ultimate transport back to the mantle in subducting oceanic lithosphere. Comparison of measured Th/U ratio to the time-integrated value derived from Pb isotopes can be used to infer whether the measured Th/U ratio was set after deposition (due to post-depositional weathering) or whether it was inherited from the preexisting crust that the ice sheets eroded. Note that weathering under anoxic conditions, such as those expected in the Mesoarchean and at least part of the Paleoproterozoic ice ages, will not alter the Th/U and therefore cannot be explored using Pb isotopes unless this weathering occurred *in situ* hundreds of millions of years later under oxidizing conditions.

A comparison of the measured and time integrated Th/U ratios is shown in Fig. 5. About half of the Neoproterozoic samples, including those from the Nantuo Formation (for which a Li isotope profile was measured), show significantly higher time integrated Th/U ratios than their measured instantaneous ratios. This is consistent with their inheriting a high Th/U from the preexisting crust that the ice sheets eroded and is inconsistent with uranium loss occurring during post-depositional weathering. The lack of elevated Th/U in most of the Paleoproterozoic samples deposited after the GOE is also consistent with their weathering signature having developed either during glaciation (which is unlikely for the reasons previously stated) or having inherited it from the preexisting crust. However, three out of five of the Duitschland samples, along with several of the analyzed samples of the Paleozoic Dwyka Group in South Africa and the two samples analyzed from the Neoproterozoic Konnarock Formation in Virginia, show moderately higher measured Th/U ratios than their time-integrated values. This implies that uranium was lost after deposition for these samples. Given the lack of paleosols or other macroscopic signs of post-depositional weathering, and the lack of correlation between U loss and indicators of weathering (e.g., CIA, Sr/Sr^*, δ^7Li, Table 1), we suggest that the weathering signature was not influenced by the process(es) responsible for removing uranium, which may have been related to post-depositional circulation of oxidized fluids. Moreover, two of the Duitschland samples (one from each of the two drill cores) fall on the 1:1 line in Fig. 5,

implying that their high Th/U was inherited from the provenance of the glacial sediments. These two samples bracket the δ^7Li and CIA values of the formation, indicating that the weathering signature in the Duitschland diamictite, which was deposited pre-GOE based on mass-independent fractionation of sulfur isotopes (Guo et al., 2009), was inherited from an UCC that had experienced strongly oxidative weathering.

The apparent Pb–Pb isochron formed by four of the five Duitschland and all of the Makganyene samples merits special comment. If the linear array is indeed an isochron with an age of 1.94 Ga, it means that both the Makganyene and Duitschland experienced the same open system behavior with regards to U and/or Pb some 300 million years after their deposition. These two stratigraphic units were deposited more than 400 km apart in separate subbasins of the Transvaal Supergroup, but the slightly younger Timeball Hill diamictite, which directly overlies the Duitschland and was sampled from one of the same drill cores, does not plot on or near the apparent isochron. If the Duitschland and Makganyene Formations experienced a major episode of metamorphism or fluid circulation at 1.94 Ga (which is otherwise not known in the local geologic record), the Timeball Hill Formation should have also experienced this event. Consequently, a more likely explanation for the line formed by the Makganyene and Duitschland Formations on the Pb isotope plots is that it represents mixing between a highly radiogenic Pb source and a crustal source with more typical Pb. These sources would derive from distinct lithologies that were eroded and mixed during the glaciation, with the more radiogenic source being a high U/Pb lithology such as a black shale. In either case, the interpretation of the time-integrated Th/U for these units is not affected. If we assume that U was mobilized at 1.94 and calculate a time-integrated Th/U ratio with this date instead of the depositional age of 2.3 Ga, the mismatch between the time-integrated and measured Th/U ratios of the three Duitschland samples is still present, as is the agreement between the two types of Th/U ratios in the Makganyene Formation.

In summary, if our conclusions above are correct that the origin of the weathering signature in the majority of the glacial diamictites reflects their provenance, then these deposits provide a window into past weathering conditions on the continents dating back to the Archean. We now explore the use of diamictites, coupled with the weathering signature recorded in other fine-grained clastic sediments to track the weathering history of the continental crust.

6.3. Continental weathering through time

The glacial diamictites provide a record of the average weathering intensity of the UCC that the ice sheets sampled. Given that regional influences may dominate (e.g., the strong A-type granite signature of the Neoproterozoic deposits from the Pocatello Formation, Idaho, Gaschnig et al., 2014), and that weathering intensity is expected to be a function of geography (greater in the tropics and less intense towards the poles), it is desirable to obtain samples from a wide geographic distribution for a given time period in order to make inferences about how weathering intensity might have changed through time. For the diamictites, some glacial intervals yield more widely distributed deposits than others. For example, the Phanerozoic, Neoproterozoic, and Paleoproterozoic glacial diamictites cover broad geographic regions, but Archean deposits are confined to South Africa. To address this concern about geographic coverage of the diamictites, we also incorporate Li data for shales and loess in our evaluation.

Both shales and loess sample large geographical areas and are the products of mixing and homogenizing effects, allowing them to be used to derive averages of the composition of the upper continental crust and trace the weathering intensity of the source regions (Taylor et al., 1983a,b; Gallet et al., 1996; Gallet et al., 1998; Teng et al., 2004; Hessler and Lowe, 2006; Qiu et al., 2009; Sauzéat et al., 2015). Loess, wind-blown sediment consisting mainly of silt-sized particles with a minor amount of clay minerals, derives from both glacial outwash and desert regions. Glacial loess particles are produced by mechanical abrasion by glaciers, thus limiting chemical weathering (Smalley and Cabrera, 1970; Gallet et al., 1996; Teng et al., 2004). On the downside, loess deposits are available only in the Pleistocene. By contrast, shales occur throughout most of Earth history.

New major element and δ^7Li data for thirty-four Archean and Paleoproterozoic shales from South Africa (Appendix Table A6-1), are combined with literature data for shales and fine-grained terrigenous sediments of all ages (see Appendix Tables A6-1 and A6-2), and the data for the glacial diamictites from this study to evaluate the weathering conditions prevalent through Earth history. We group the samples into the "Archean + Paleoproterozoic" and " Post-Paleoproterozoic" time periods (Fig. 6). As shown in Figs. 1 and 6, the shales and glacial diamictites of a given time period generally show the same weathering intensity (for example, post-Paleoproterozoic diamictites, shales, and loess have similar average CIA of 62 ± 12 (2σ), 69 ± 20 (2σ) and 61 ± 8 (2σ), respectively, and δ^7Li values of -0.1 ± 3.6 (2σ), $+0.5 \pm 4.8$ (2σ), and $+0.6 \pm 4.1$ (2σ), respectively). One can see that the Archean + Paleoproterozoic samples' CIA (old group CIA) is skewed to higher values than that of the Post-Paleoproterozoic group (young group CIA) (Fig. 6a and c), and the older group also has slightly lower δ^7Li values (Fig. 6b and d).

In order to determine whether the shales, loess and glacial diamictites from a given time period carry similar weathering signatures and if the weathering intensity has changed significantly through time, we have run Student's *t*-tests using the *ttest2.m* function in Matlab (while setting the null hypothesis at the default 5% significant level) on the available data (see Appendix for details). We first ran the Student's *t* test for glacial diamictites and shales (and loess, where available) for a given time period to determine whether these data sets carry comparable weathering signatures (Appendix Table A7). The δ^7Li *t*-test results for both older samples (Archean + Paleoproterozoic) and younger samples show that glacial diamictites and shales have statistically indistinguishable δ^7Li values. But the CIA *t*-test results show that shales have a higher average CIA (i.e.,

76 for old shales and 68 for young shales) than that of glacial diamictites (i.e., 69 for old tillites and 62 for young tillites). This result may reflect the fact that far fewer CIA data exist for glacial diamictites than for shales, or it may reflect a greater weathering intensity in the shale data (see Appendix).

We now combine the diamictite and other sedimentary rock data to determine whether different time periods are statistically distinguishable in terms of weathering intensity (Appendix Tables A8 and A9). Although the δ^7Li values for the older and younger tillites are statistically indistinguishable, their CIA values are statistically distinct, and both measures of weathering intensity are statistically distinct between the older and younger shales (Appendix Table A8). For the combined dataset, both δ^7Li and CIA vary with time, from 3400 to 0.01 Ma (Fig. 7, data sources in Appendix Tables A6-1 and A6-2). The δ^7Li values show a slight increase from Archean to Phanerozoic, whereas the CIA values exhibit an obvious and steady decrease over time, with a combined average of 80 for the Archean, 72 for the Proterozoic (including a decrease within the Proterozoic from the Paleoproterozoic: 74, Mesoproterozoic: 74, to Neoproterozoic: 68), and 66 in the Phanerozoic. These trends suggest a decrease in chemical weathering intensity through time and are consistent with previous studies. For example, Condie et al. (2001) described a secular decrease of the CIA of shales through Earth's history from an average of ~80 during the Archean, through ~75 in the Proterozoic, to ~70 for average Phanerozoic shales. Gonzalez-Alvarez and Kerrich (2012) examined the CIA trend in diverse sedimentary rocks from the Precambrian and found CIA ~80 to 100 in the Mesoarchean, ~80 to 90 in the Neoarchean, and ~70 to 85 in the Proterozoic. All of these results suggest more intense weathering of subaerially exposed rocks during the Archean, which is likely related to climatic conditions.

The nature of Archean climate is ambiguous because of the dearth of terrigenous sedimentary deposits, and climate modeling yields different results, ranging from a 'hot-house' to a 'cold-house'. A hot greenhouse has been suggested for the Archean period, attended by intense rainfall and surface temperatures as high as ~85 °C (Knauth and Lowe, 2003; Hessler and Lowe, 2006) due to inferred high Pco_2 (100–1000 times higher than modern level) (Walker, 1986; Kasting and Ackerman, 1986; Kasting, 1987, 1993). However, high Pco_2 in the Archean has been questioned by Rye et al. (1995), who suggested that other greenhouse gases, in addition to CO_2, existed in the Archean atmosphere. Others propose that global warming was facilitated in the Archean by a muted cosmic ray flux (CRF), which reduced cloud cover and lowered planetary albedo (Veizer, 2005; Eyles, 2007). On the other hand, some favor a cold Archean climate due to the "faint young sun" that had an output 25–30% lower than that of today (Caldeira and Kasting, 1992; Zahnle and Sleep, 2002). Kasting and Howard (2006) proposed a more temperate warm Archean Earth somewhere between the hot and cold Archean models. Eyles (2007) questioned the cold Archean model because of the lack of widespread glacial deposits. Furthermore, a cold Archean climate model is difficult to reconcile with evidence for intense weathering in the Archean, which has been suggested in several previous studies (Wronkiewicz and Condie, 1987; Corcoran and Mueller, 2004; Hessler and Lowe, 2006; Heinrich, 2015) and corroborated here.

Our result is consistent with severe weathering conditions prevailing during the Archean, suggesting warm temperatures and humid, possibly acidic soil conditions. Weathering is facilitated by warmer surface temperatures as chemical reaction rates increase exponentially with temperature (Walker et al., 1981; Retallack, 1990; White and Blum, 1995), allowing more resistant minerals to undergo hydrolysis (Hessler and Lowe, 2006). Intense and widespread rainfall would have continuously and rapidly leached the rocks with under-saturated fluids and reinforced the exponential influence of temperature on weathering (White and Blum, 1995); high Pco_2 would have made the fluids more acidic and thus increased the hydrolytic decomposition rate of minerals.

While the CIA trend with time is clear in the data for shales, tillites, and loess, the trend in δ^7Li is far from distinct. The reasons for the limited variability in δ^7Li through time may reflect the changing magnitude of Li isotope fractionation with weathering intensity. In a recent study of Li in rivers within the Amazon basin, Dellinger et al. (2015) showed that Li isotopic fractionation between water and secondary phases is largest at intermediate weathering intensity (as defined by the ratio of the chemical weathering rate to denudation rate) and is smallest at the highest (e.g., in laterite-dominated terranes) and lowest weathering intensities (e.g., in fresh igneous rock-dominated terranes). Moreover, Huh et al. (2004) showed that leaching of Li from basaltic soils in Hawaii varies with the effective cation exchange capacity, which is low under conditions of heavy rainfall (as measured by mean annual precipitation) where the soils are acidified. Thus, high weathering intensity on the Archean Earth characterized by relatively high temperatures, high rainfall and acidic conditions may have led to less Li retention in the regolith and limited isotopic fractionation, consistent with our observations.

In summary, both δ^7Li values of shales and CIA values for tillites, shales and loess show a statistically robust change through time suggestive of more intense weathering in the Archean, though the changes in CIA are of greater magnitude than those of δ^7Li. Such changes are consistent with previous suggestions of a more intense weathering regime during the Archean (e.g., Fedo et al., 1996; Sugitani et al., 1996; Corcoran et al., 1998; Donaldson and de Kemp, 1998; Bhat and Ghosh, 2001; Condie et al., 2001; Corcoran and Mueller, 2004; Hessler and Lowe, 2006; Heinrich, 2015).

7. CONCLUSIONS

The fine-grained matrix of nearly all sampled glacial diamictites, from five glacial intervals spanning 2.9 billion years of Earth history, carry a strong chemical weathering signature. This signature is mainly inherited from the upper continental crust over which the glaciers traversed, based on the lack of chemically or visually recognizable weather-

ing horizons and on Pb isotopic systematics. Our data consequently provide insights into the weathering conditions of ancient continents and weathering intensity through time. Intense weathering signals are observed in Mesoarchean and Paleoproterozoic South African glacial diamictites, but the Mesoarchean glacial diamictites are limited to the South African region; therefore we cannot be certain if the intense weathering signature is a regional or global phenomenon. Both strong and weak weathering signatures were found in Paleoproterozoic South African and North American diamictites, respectively. Neoproterozoic and Phanerozoic glacial diamictites record generally weaker weathering signals compared to Archean and Paleoproterozoic diamictites. The decreasing CIA and slightly increasing δ^7Li from the Archean to Phanerozoic recorded in glacial diamictites, shales and loess reflect decreasing intensity of chemical weathering through time, consistent with previous suggestions that high rainfall, high temperature and high CO_2 during the Archean may have contributed to a more aggressive weathering environment.

ACKNOWLEDGMENTS

This research was supported by NSF Grants EAR-0948549, EAR-1321954, and FESD EAR-1338810. We thank Shan Gao and a grant from the State Key Laboratory of Geological Processes and Mineral Resources at China University of Geosciences in Wuhan for additional support for field work; Jay Kaufman, Nic Beukes, Charlie Hoffmann, Kang Chen, Yongsheng Liu, Lian Zhou, and Zhaochu Hu for assistance in the field; Will Junkin and Michael Ream for help with sample preparation of the diamictites, and Claire Zurkowski for help in analyzing the shales; Richard Ash and Igor Puchtel for their assistance in the Plasma Lab and Clean Lab at the University of Maryland, College Park; Tim Mock, Rick Carlson, and Steve Shirey for their analytical help and hospitality at DTM; and Lucie Sauzéat for providing a preprint of her paper on loess. We are grateful to Sydney Hemming for supplying the Greenland glacial sediment, Anne Jennings for supplying the Hudson Straight sediments, Heidi Anderson for providing the Bolivian diamictites, Kent Condie, David Wronkiewicz and Bradley Guy for supplying the Archean and Paleoproterozoic shales. We appreciate Ming Tang's help in guiding Su Li through the Li isotope method, Xiao-Ming Liu, Allison Greaney, Mark Larson and Harrison Lisabeth provided helpful comments on earlier versions of this paper. Su Li benefited from the valuable opportunities and facilities provided by the China Scholarship Council and Prof. Yaoqi Zhou at China University of Petroleum. Finally, we greatly appreciate the editorial work of Brian W. Stewart, and the detailed comments from two anonymous reviewers.

APPENDIX A. SUPPLEMENTARY DATA

Supplementary data associated with this article can be found, in the online version, at http://dx.doi.org/10.1016/j.gca.2015.12.012.

REFERENCES

Albarède F. (1998) The growth of continental crust. *Tectonophysics* **296**, 1–14.

Allen P. A., Bowring S., Leather J., Brasier M., Cozzi A., Grozinger J. P., McCarrron G. and Amthor J. J. (2002) Chronology of neoproterozoic glaciations: new sights from Oman. In *16th International Sedimentological Congress, Rand Afrikaans University, Jobannesburg, South Africa*, pp. 7–8. 16th International Sedimentological Congress, Rand Afrikaans University, Jobannesburg, South Africa.

Bekker A., Kaufman A. J., Karhu J. A., Beukes N. J., Swart Q. D., Coetzee L. L. and Eriksson K. A. (2001) Chemostratigraphy of the Paleoproterozoic Duitschland Formation, South Africa: implications for coupled climate change and carbon cycling. *Am. J. Sci.* **301**, 261–285.

Bhat M. I. and Ghosh S. K. (2001) Geochemistry of the 2.51 Ga old Rampur group pelites, western Himalayas: implications for their provenance and weathering. *Precambr. Res.* **108**, 1–16.

Bouman C., Elliott T. and Vroon P. Z. (2004) Lithium inputs to subduction zones. *Chem. Geol.* **212**, 59–79.

Caldeira K. and Kasting J. F. (1992) Susceptibility of the early Earth to irreversible glaciation caused by carbon dioxide clouds. *Nature* **359**, 226–228.

Canil D. and Lacourse T. (2011) An estimate for the bulk composition of juvenile upper continental crust derived from glacial till in the North American Cordillera. *Chem. Geol.* **284** (3–4), 229–239.

Caputo M. V. and Crowell J. C. (1985) Migration of glacial centers across Gondwana during the Paleozoic Era. *Geol. Soc. Am. Bull.* **96**, 1020–1036.

Castro A., Corretge L. G. and EI-Biad M. (1999) Origin of peraluminous granites and granodiorites, Iberian massif, Spain: an experimental test of granite petrogenesis. *Contrib. Mineral. Petrol.* **135**, 255–276.

Chan L.-H. and Edmond J. M. (1988) Variation of lithium isotope composition in the marine environment: a preliminary report. *Geochim. Cosmochim. Acta* **52**, 1711–1717.

Chan L. H., Edmond J. M., Thompson G. and Gillis K. (1992) Lithium isotopic composition of submarine basalts: implications for the lithium cycle in the oceans. *Earth Planet. Sci. Lett.* **108**, 151–160.

Chan L. H., Leeman W. P. and Plank T. (2006) Lithium isotopic composition of marine sediments. *Geochem. Geophys. Geosyst.* **7**(6), 1–25.

Collerson K. D. and Kamber B. S. (1999) Evolution of the continents and the atmosphere inferred from Th–U–Nb systematics of the depleted mantle. *Science* **283**, 1519–1522.

Condie K. C. (1993) Chemical composition and evolution of the upper continental crust: contrasting results from surface samples and shales. *Chem. Geol.* **104**, 1–37.

Condie K. C., Des Marais D. J. and Abbott D. (2001) Precambrian superplumes and supercontinents: a record in black shales, carbon isotopes, and paleoclimates? *Precambr. Res.* **106**, 239–260.

Condon D., Zhu M. Y., Bowring S., Wang W., Yang A. and Jin Y. G. (2005) U–Pb ages from the neoproterozoic doushantuo formation, China. *Science* **308**, 95–98.

Corcoran P. L. and Mueller W. U. (2004) Aggressive Archean weathering. In *The Precambrian Earth: Tempos and Events* (eds. P. G. Eriksson, W. Altermann, D. R. Nelson, W. U. Mueller and O. Catuneanu). Elsevier, New York, pp. 494–504.

Corcoran P. L., Mueller W. U. and Chown E. H. (1998) Climatic and tectonic influences on fan deltas and wave- to tide-controlled shoreface deposits: evidence from the Archaean Keskarrah Formation, Slave Province, Canada. *Sed. Geol.* **120**, 125–152.

Crowell J. C. (1978) Gondwanan glaciation, cyclothems, continental positioning, and climate change. *Am. J. Sci.* **278**, 1345–1372.

Crowell J. C. (1999) Pre-mesozoic ice ages: their bearing on understanding the climate system. *Geol. Soc. Am. Memoirs* **192**, 1–112.

Cuccuru S., Casini L., Oggiano G. and Cherchi G. P. (2012) Can weathering improve the toughness of a fractured rock? A case study using the San Giacomo granite. *Bull. Eng. Geol. Environ.* **71**, 557–567.

Dellinger M., Gaillardet J., Bouchez J., Calmels D., Galy V., Hilton R. G., Louvat P. and France-Lanord C. (2014) Lithium isotopes in large rivers reveal the cannibalistic nature of modern continental weathering and erosion. *Earth Planet. Sci. Lett.* **401**, 359–372.

Dellinger M., Gaillardet J., Bouchez J., Calmels D., Louvat P., Dosseto A., Gorge C., Alanoca L. and Maurice L. (2015) Riverine Li isotope fractionation in the Amazon River basin controlled by the weathering regimes. *Geochim. Cosmochim. Acta* **164**, 71–93.

Donaldson J. A. and de Kemp E. A. (1998) Archaean quartz arenites in the Canadian Shield: examples from the Superior and Churchill Provinces. *Sed. Geol.* **120**, 153–176.

Donskaya T. V., Gladkochub D. P., Pisarevsky S. A., Poller U., Mazukabzov A. M. and Bayanova T. B. (2009) Discovery of Archaean crust within the Akitkan orogenic belt of the Siberian craton: new insight into its architecture and history. *Precambr. Res.* **170**, 61–72.

Eade K. E. and Fahrig W. F. (1973) *Regional, lithological, and temporal variation in the abundances of some trace elements in the Canadian Shield*.

Elliott T., Thomas A., Jeffcoate A. and Niu Y.-L. (2006) Lithium isotope evidence for subduction-enriched mantle in the source of mid-ocean-ridge basalts. *Nature* **443**, 565–568.

Eyles N. (2007) Glacio-epochs and the supercontinent cycle after ~3.0 Ga: tectonic boundary conditions for glaciation. *Palaeogeogr. Palaeoclimatol. Palaeoecol.* **258**, 89–129.

Fedo C. M., Eriksson K. A. and Krogstad E. J. (1996) Geochemistry of shales from the Archean (~3.0 Ga) Buhwa Greenstone Belt, Zimbabwe: implications for provenance and source-area weathering. *Geochim. Cosmochim. Acta* **60**(10), 1751–1763.

Frimmel H. E., Klotzli U. S. and Siegfried P. R. (1996) New Pb–Pb single zircon age constraints on the timing of Neoproterozoic glaciation and continental break-up in Namibia. *J. Geol.* **104**, 459–469.

Galer S. J. G. and Abouchami W. (1998) Practical application of lead triple spiking for correction of instrumental mass discrimination. *Mineral. Mag.* **62A**, 491–492.

Gallet S., Jahn B. M. and Torii M. (1996) Geochemical characterization of the Luochuan loess-paleosol sequence, China, and paleoclimatic implications. *Chem. Geol.* **133**, 67–88.

Gallet S., B-m Jahn., Lanoe V. V., Dia A. and Rossello E. (1998) Loess geochemistry and its implications for particle origin and composition of the upper continental crust. *Earth Planet. Sci. Lett.* **156**, 157–172.

Gao S., Luo T. C., Zhang B. R., Zhang H. F., Han Y. W., Zhao Z. D. and Hu Y. K. (1998) Chemical composition of the continental crust as revealed by studies in East China. *Geochim. Cosmochim. Acta* **62**(11), 1959–1975.

Gaschnig R. M., Rudnick R. L., McDonough W. F., Kaufman A. J., Hu Z. C. and Gao S. (2014) Onset of oxidative weathering of continents recorded in the geochemistry of ancient glacial diamictites. *Earth Planet. Sci. Lett.* **408**, 87–99.

Gaschnig R. M., Rudnick R. L., McDonough W. F., Kaufman A. J., Vervoort J. D. and Fisher C. M. (2015) *Insights on crustal growth from detrital zircons in ancient glacial deposits*.

Gonzalez-Alvarez I. and Kerrich R. (2012) Weathering intensity in the Mesoproterozoic and modern large-river systems: a comparative study in the Belt-Purcell Supergroup, Canada and USA. *Precambr. Res.* **208–211**, 174–196.

Goldschmidt V. M. (1933) Grundlagen der quantitativen geochemie. *Fortschritte der Mineralogie, Krystallographie und Petrographie* **17**, 112.

Gong Q. J., Deng J., Wang C. M., Wang Z. L. and Zhou L. Z. (2013) Element behaviors due to rock weathering and its implication to geochemical anomaly recognition: a case study on Linglong biotite granite in Jiaodong peninsula, China. *J. Geochem. Explor.* **128**, 14–24.

Guo Q. J., Strauss H., Kaufman A. J., Schröder S., Gutzmer J., Wing B., Baker M. A., Bekker A., Jin Q. S., Kim S.-T. and Farquhar J. (2009) Reconstructing Earth's surface oxidation across the Archean-Proterozoic transition. *Geology* **37**(5), 399–402.

Hambrey M. J. (1985) The late Ordovician-early Silurian glacial period. *Palaeogeogr. Palaeoclimatol. Palaeoecol.* **51**, 273–289.

Hathorne E. C. and James R. H. (2006) Temporal record of lithium in seawater: a tracer for silicate weathering? *Earth Planet. Sci. Lett.* **246**, 393–406.

Heinrich C. A. (2015) Witwatersrand gold deposits formed by volcanic rain, anoxic rivers and Archean life. *Nature*, 1–4.

Hessler A. M. and Lowe D. R. (2006) Weathering and sediment generation in the Archean: an integrated study of the evolution of siliciclastic sedimentary rocks of the 3.2 Ga Moodies Group, Barberton greenstone belt, South Africa. *Precambr. Res.* **151**, 185–210.

Hoffman P. F. and Li Z. X. (2009) A palaeogepgraphy context for Neoproterozoic glaciation. *Palaeogeogr. Palaeoclimatol. Palaeoecol.* **277**, 158–172.

Huang Y., Chubakov V., Mantovani F., Rudnick R. L. and McDonough W. F. (2013a) A reference Earth model for the heat-producing elements and associated geoneutrino flux. *Geochem. Geophys. Geosyst.* **14**, 2003–2029.

Huang H., Polat A. and Fryer B. J. (2013b) Origin of Archean tonalite–trondhjemite–granodiorite (TTG) suites and granites in the Fiskenæsset region, southern West Greenland: implications for continental growth. *Gondwana Res.* **23**, 452–470.

Huang Y., Chubakov V., Mantovani F., Rudnick R. L. and McDonough W. F. (2013c) A reference Earth model for the heat-producing elements and associated geoneutrino flux. *Geochem. Geophys. Geosyst.* **14**, 1525–2027.

Hu Z. and Gao S. (2008) Upper crustal abundances of trace elements: a revision and update. *Chem. Geol.* **253**, 205–221.

Huh Y., Chan L.-H., Zhang L. and Edmond J. M. (1998) Lithium and its isotopes in major world rivers: implications for weathering and the oceanic budget. *Geochim. Cosmochim. Acta* **62**, 2039–2051.

Huh Y., Chan L. H. and Edmond J. M. (2001) Lithium isotopes as a probe of weathering processes: Orinoco River. *Earth Planet. Sci. Lett.* **194**(1–2), 189–199.

Huh Y., Chan L.-H. and Chadwick O. A. (2004) Behavior of lithium and its isotopes during weathering of Hawaiian basalt. *Geochem. Geophys. Geosyst.* **5**, Q09002. http://dx.doi.org/10.1029/2004GC000729.

James R. H. and Palmer M. R. (2000) The lithium isotope composition of international rock standards. *Chem. Geol.* **166**, 319–326.

Jacobsen A. D. and Blum J. D. (2000) Ca/Sr and $^{87}Sr/^{86}Sr$ geochemistry of disseminated calcite in Himalayan silicate rocks from Nanga Parbat: influence on river-water chemistry. *Geology* **28**(5), 463–466.

Jochum K. P., Nohl U., Herwig K., Lammel E., Stoll B. and Hofmann A. W. (2005) GeoReM: a new geochemical database for reference materials and isotopic standards. *Geostand. Geoanal. Res.* **29**(3), 333–338.

Kasting J. F. and Ackerman T. P. (1986) Climatic consequences of very high-carbon dioxide levels in the Earth's early atmosphere. *Science* **234**, 1383–1385.

Kasting J. F. (1987) Theoretical constraints on oxygen and carbon-dioxide concentrations in the Precambrian atmosphere. *Precambr. Res.* **34**, 205–229.

Kasting J. F. (1993) Earth's early atmosphere. *Science* **259**, 920–926.

Kasting J. F. and Howard M. T. (2006) Atmospheric composition and climate on the early Earth. *Philos. Trans. R. Soc. B* **361**, 1733–1742.

Kisakürek B., Widdowson M. and James R. H. (2004) Behavior of Li isotopes during continental weathering: the Bidar laterite profile, India. *Chem. Geol.* **212**, 27–44.

Kisakürek B., James R. H. and Harris N. B. W. (2005) Li and δ^7Li in Himalayan rivers: proxies for silicate weathering? *Earth Planet. Sci. Lett.* **237**, 387–401.

Knauth L. P. and Lowe D. R. (2003) High Archean climatic temperature inferred from oxygen isotope geochemistry of cherts in the 3.5 Ga Swaziland Supergroup, South Africa. *Geol. Soc. Am. Bull.* **115**, 566–580.

Kopp R. E., Kirschvink J. L., Hilburn L. A. and Nash C. Z. (2005) The Paleoproterozoic snowball Earth: a climate disaster triggered by the evolution of oxygenic photosynthesis. *Proc. Natl. Acad. Sci. U.S.A.* **102**, 11131–11136.

Krogstad E. J., Fedo C. M. and Eriksson K. A. (2004) Provenance ages and alteration histories of shales from the Middle Archean Buhwa greenstone belt, Zimbabwe: Nd and Pb isotopic evidence. *Geochim. Cosmochim. Acta* **68**, 319–332.

Lee C. T. A., Morton D. M., Little M. G., Kistler R., Horodyskyj U. N., Leeman W. P. and Agranier A. (2008) Regulating continent growth and composition by chemical weathering. *Proc. Nat. Acad. Sci. U.S.A.* **105**, 4981–4986.

Lemarchand E., Chabaux F., Vigier N., Millot R. and Pierret M. C. (2010) Lithium isotope systematics in a forested granitic catchment (Strengbach, Vosges Mountains, France). *Geochim. Cosmochim. Acta* **74**, 4612–4628.

Li G. J. and West A. J. (2014) Evolution of Cenozoic seawater lithium isotopes: coupling of global denudation regime and shifting seawater sinks. *Earth Planet. Sci. Lett.* **401**, 284–293.

Liu X.-M. and Rudnick R. L. (2011) Constraints on continental crustal mass loss via chemical weathering using lithium and its isotopes. *Proc. Natl. Acad. Sci. U.S.A.* **108**, 20873–20880.

Liu S. A., Teng F. Z., He Y. S., Ke S. and Li S. G. (2010) Investigation of magnesium isotope fractionation during granite differentiation: implication for Mg isotopic composition of the continental crust. *Earth Planet. Sci. Lett.* **297**, 646–654.

Liu X.-M., Rudnick R. L., McDonough W. F. and Cummings M. L. (2013) Influence of chemical weathering on the composition of the continental crust: insights from Li and Nd isotopes in bauxite profiles developed on Columbia River Basalts. *Geochim. Cosmochim. Acta* **115**, 73–91.

Liu X.-M., Wanner C., Rudnick R. L. and McDonough W. F. (2015) Processes controlling δ^7Li in rivers illuminated by study of streams and ground waters draining basalts. *Earth Planet. Sci. Lett.* **409**, 212–224.

Lund K., Aleinikoff J. N., Evans K. V. and Fanning C. M. (2003) SHRIMP U–Pb geochronology of Neoproterozoic Windermere Supergroup, central Idaho: implications for rifting of western laurentia and synchroneity of Sturtian glacial deposits. *Geol. Soc. Am. Bull.* **115**, 349–372.

Magna T., Janousek V., Kohut M., Oberli F. and Wiechert U. (2010) Fingerprinting sources of orogenic plutonic rocks from Variscan belt with lithium isotopes and possible link to subduction-related origin of some A-type granites. *Chem. Geol.* **2010**(274), 94–107.

Manikyamba C. and Kerrich R. (2006) Geochemistry of Black shales from the Neoarchean Sandur Superterrane, India: first cycle volcanogenic sedimentary rocks in an intraoceanic arc-trench complex. *Geochim. Cosmochim. Acta* **70**, 4663–4679.

McDonough W. F. (1990) Constraints on the composition of the continental lithospheric mantle. *Earth Planet. Sci. Lett.* **101**, 1–18.

McDonough W. F. and Sun S.-S. (1995) Composition of the Earth. *Chem. Geol.* **120**, 223–253.

McLennan S. M. and Taylor S. R. (1980) Th and U in sedimentary rocks: crustal evolution and sedimentary recycling. *Nature* **285**, 621–624.

McLennan S. M., Hemming S. R., Taylor S. R. and Eriksson K. A. (1993) Early Proterozoic crustal evolution: geochemical and Nd-Pb isotopic evidence from metasedimentary rocks, southwestern North America. *Geochim. Cosmochim. Acta* **59**, 1153–1177.

Melezhik V. A., Young G. M., Eriksson P. G., Altermann W., Kump L. R. and Lepland A. (2013) Huronian-age glaciation. In *Global Events and the Fennoscandian Arctic Russia – Drilling Early Earth Project. Reading the Archive of Earth's Oxygenation*, vol. 3 (eds. V. A. Melezhik, R. Prave, E. J. Hanski, A. E. Fallick, A. Lepland, L. R. Kump and H. Strauss), pp. 1059–1109.

Millot R., Guerrot C. and Vigier N. (2004) Accurate and high-precision measurement of lithium isotopes in two reference materials by MC-ICP-MS. *Geostand. Geoanal. Res.* **28**(1), 153–159.

Millot R., Vigier N. and Gaillardet J. (2010) Behaviour of lithium and its isotopes during weathering in the Mackenzie Basin, Canada. *Geochim. Cosmochim. Acta* **74**, 3897–3912.

Misra S. and Froelich P. N. (2012) Lithium isotope history of Cenozoic seawater: changes in silicate weathering and reverse weathering. *Science* **335**, 818–823.

Moriguti T. and Nakamura E. (1998) Across-arc variation of Li isotopes in lavas and implications for crust/mantle recycling at subduction zones. *Earth Planet. Sci. Lett.* **163**, 167–174.

Moyen J. F. (2011) The composite Archean grey gneisses: petrological significance, and evidence for a non-unique tectonic setting for Archean crustal growth. *Lithos* **123**, 21–36.

Moyen J. F., Martin H. and Jayananda M. (2001) Multi-element geochemical modeling of crust-mantle interactions during late-Archean crustal growth: the Closepet granite (South India). *Precambr. Res.* **112**, 87–105.

Nesbitt H. W. and Young G. M. (1982) Early Proterozoic climates and plate motions element chemistry of lutites. *Nature* **299**, 715–717.

Nesbitt H. W. and Young G. M. (1996) Petrogenesis of sediments in the absence of chemical weathering: effects of abrasion and sorting on bulk composition and mineralogy. *Sedimentology* **43**, 341–358.

Pearce J. A., Harris N. B. W. and Tindle A. G. (1984) Trace element discrimination diagram for the tectonic interpretation of granitic rocks. *J. Petrol.* **25**, 956–983.

Pillans B. and Gibbard P. (2012) The quaternary period. In *Geological Time Scale* (eds. F. M. Gradstein, J. G. Ogg, M. D. Schmitz and G. M. Ogg). Elsevier, Amsterdam, pp. 980–1004.

Pistiner J. S. and Henderson G. M. (2003) Lithium-isotope fractionation during continental weathering processes. *Earth Planet. Sci. Lett.* **214**, 327–339.

Pogge von Strandmann P. A. E. and Henderson G. M. (2015) The Li isotope response to mountain uplift. *Geology* **43**, 67–70.

Pogge von Strandmann P. A. E., Burton K. W., James R. H., van Calsteren P., Gislason S. R. and Mokadem F. (2006) Riverine behavior of uranium and lithium isotopes in an actively glaciated basaltic terrain. *Earth Planet. Sci. Lett.* **251**, 134–147.

Pogge von Strandmann P. A. E., Burton K. W., James R. H., van Calsteren P. and Gislason S. R. (2010) Assessing the role of climate on uranium and lithium isotope behaviour in rivers draining a basaltic terrain. *Chem. Geol.* **270**, 227–239.

Pogge von Strandmann P. A. E., Opfergelt S., Lai Y. J., Sigfusson B., Gislason S. R. and Burton K. W. (2012) Lithium, magnesium and silicon isotope behavior accompanying weathering in a basaltic soil and pore water profile in Iceland. *Earth Planet. Sci. Lett.* **339–340**, 11–23.

Pogge von Strandmann P. A. E., Jenkyns H. C. and Woodfine R. G. (2013) Lithium isotope evidence for enhanced weathering during Oceanic Anoxic Event 2. *Nat. Geosci.* **6**, 668–672.

Pollack G. D., Krogstad E. J. and Bekker A. (2009) U–Th–Pb-REE systematics of organic-rich shales from the ca. 2.15 Ga Sengoma Argillite Formation, Botswana: evidence for oxidative continental weathering during the Great Oxidation Event. *Chem. Geol.* **260**, 172–185.

Qiu L. (2011) *Lithium and δ^7Li Behavior during Metamorphic Processes and Crustal Evolution*. University of Maryland.

Qiu L., Rudnick R. L., McDonough W. F. and Merriman R. J. (2009) Li and δ^7Li in mudrocks from the British Caledonides: metamorphism and source influences. *Geochim. Cosmochim. Acta* **73**, 7325–7340.

Qiu L., Rudnick R. L., Ague J. J. and McDonough W. F. (2011) A lithium isotopic study of sub-greenschist to greenschist facies metamorphism in an accretionary prism, New Zealand. *Earth Planet. Sci. Lett.* **301**, 213–221.

Rad S., Rivé K., Vittecoq B., Cerdan O. and Allègre C. J. (2013) Chemical weathering and erosion rates in the Lesser Antilles: an overview in Guadeloupe, Martinique and Dominica. *J. S. Am. Earth Sci.* **45**, 331–344.

Retallack G. J. (1990) *Soils of the Past: An Introduction to Paleopedology*. Unwin Hyman, Boston.

Rudnick R. L. (1995) Making continental crust. *Nature* **378**, 571–578.

Rudnick R. L. and Gao S. (2003) Composition of the continental crust. In *The Crust, Treatise on Geochemistry* (eds. R. L. Rudnick, D. H. Heinrich and K. T. Karl). Pergamon, Oxford, pp. 1–64.

Rudnick R., Tomascak P. B., Njo H. B. and Gardner R. (2004) Extreme lithium isotopic fractionation during continental weathering revealed in saprolites from South Carolina. *Chem. Geol.* **212**, 45–57.

Rye R., Kuo P. H. and Holland H. D. (1995) Atmospheric carbon-dioxide concentrations before 2.2 billion years ago. *Nature* **378**, 603–605.

Sauzéat L., Rudnick R. L., Chauvel C., Garcon M. and Tang M. (2015) New perspective on the Li isotopic composition of the upper continental crust and its weathering signature. *Earth Planet. Sci. Lett.* **428**, 181–192.

Seixas L. A. R., David J. and Stevenson R. (2012) Geochemistry, Nd isotopes and U–Pb geochronology of a 2350 Ma TTG suite, Minas Gerais, Brazil: implications for the crustal evolution of the southern São Francisco craton. *Precambr. Res.* **196–197**, 61–80.

Smalley I. J. and Cabrera J. G. (1970) The shape and surface texture of loess particles. *Geol. Soc. Am. Bull.* **81**, 1591–1595.

Stacey J. S. and Kramers J. D. (1975) Approximation of terrestrial lead isotope evolution by a two-stage model. *Earth Planet. Sci. Lett.* **26**, 207–221.

Sugitani K., Horiuchi Y., Adachi M. and Sugisaki R. (1996) Anomalously low $A1_2O_3/TiO_2$ values for Archean cherts from the Pilbara Block, Western Australia possible evidence for extensive chemical weathering on the early earth. *Precambr. Res.* **80**, 49–76.

Taylor S. R. and Mclennan S. M. (1985) *The Continental Crust: Its Composition and Evolution*. Blackwell, Oxford.

Taylor S. R., Mclennan S. M. and Mcculloch M. T. (1983a) Geochemistry of loess, continental crustal composition and crustal model ages. *Geochim. Cosmochim. Acta.* **47**, 1897–1905.

Taylor S. R., Mclennan S. M. and McCulloch M. T. (1983b) Geochemistry of loess, continental crustal composition and crustal model ages. *Geochim. Cosmochim. Acta* **47**, 1897–1905.

Teng F. Z., Mcdonough W. F., Rudnick R. L., Dalpe C., Tomascak P. B., Chappell B. W. and Gao S. (2004) Lithium isotopic composition and concentration of the upper continental crust. *Geochim. Cosmochim. Acta* **68**, 4167–4178.

Teng F. Z., McDonough W. F., Rudnick R. L., Walker R. J. and Sirbescu M. L. C. (2006) Lithium isotopic systematic of granites and pegmatites from the Black Hills, South Dakota. *Am. Mineral.* **91**, 1488–1498.

Teng F. Z., Rudnick R. L., McDonough W. F., Gao S., Tomascak P. B. and Liu Y. S. (2008) Lithium isotopic composition and concentration of the deep continental crust. *Chem. Geol.* **255**, 47–59.

Teng F. Z., Rudnick R. L., McDonough W. F. and Wu F. Y. (2009) Lithium isotopic systematics of A-type granites and their mafic enclaves: further constraints on the Li isotopic composition of the continental crust. *Chem. Geol.* **262**, 415–424.

Teng F. Z., Li W. Y., Rudnick R. L. and Gardner L. R. (2010) Contrasting lithium and magnesium isotope fractionation during continental weathering. *Earth Planet. Sci. Lett.* **300**, 63–71.

Tomascak P. B., Langmuir C. H., le Roux P. J. and Shirey S. B. (2008) Lithium isotopes in global mid-ocean ridge basalts. *Geochim. Cosmochim. Acta* **72**, 1626–1637.

Veizer J. (2005) Celestial climate driver: a perspective from four billion years of the carbon cycle. *Geosci. Can.* **32**, 13–28.

Vigier N., Gislason S. R., Burton K. W., Millot R. and Mokadem F. (2009) The relationship between riverine lithium isotope composition and silicate weathering rates in Iceland. *Earth Planet. Sci. Lett.* **287**, 434–441.

Vigier N. and Goddéris Y. (2015) A new approach for modeling Cenozoic oceanic lithium isotope paleo-variations: the key role of climate. *Clim. Past.* **11**, 635–645.

Visser J. N. J. (1982) Upper Carboniferous glacial sedimentation in the Karoo Basin near Prieska, South Africa. *Palaeogeogr. Palaeoclimatol. Palaeoecol.* **38**(1–2), 63–92.

Walker J. C. G., Hays P. B. and Kasting J. F. (1981) A negative feedback mechanism for the long-term stabilization of Earth's surface temperature. *J. Geophys. Res.* **86**, 9776–9782.

Walker J. C. G. (1986) Carbon dioxide on the early Earth. *Origins Life* **16**, 117–127.

Wang Q. L., Chetelat B., Zhao Z. Q., Ding H., Li S. L., Wang B. L., Li J. and Liu X. L. (2015) Behavior of lithium isotopes in the Changjiang River system: sources effects and response to weathering and erosion. *Geochim. Cosmochim. Acta* **151**, 117–132.

Wanner C., Sonnenthal E. and Liu X.-M. (2014) Seawater δ^7Li: A direct proxy for global CO_2 consumption by continental silicate weathering? *Chem. Geol.* **381**, 154–167.

Weis D., Kieffer B., Maerschalk C., Barling J., de Jong J., Williams G. A., Hanano D., Pretorius W., Mattielli N., Scoates J. S., Goolaerts A., Friedman R. M. and Mahoney J. B. (2006) High-precision isotopic characterization of USGS reference materials by TIMS and MC-ICP-MS. *Geochem. Geophys. Geosyst.* **7**(8), Q08006.

White A. F. and Blum A. E. (1995) Effects of climate on chemical weathering in watersheds. *Geochim. Cosmochim. Acta* **59**, 1729–1747.

Williams L. B. and Hervig R. L. (2005) Lithium and boron isotopes in illite-smectite: the importance of crystal size. *Geochim. Cosmochim. Acta* **69**, 5705–5716.

Wimpenny J., Gislason S. R., James R. H., Gannoun A., Pogge Von Strandmann P. A. E. and Burton K. W. (2010a) The behavior of Li and Mg isotopes during primary phase dissolution and secondary mineral formation in basalt. *Geochim. Cosmochim. Acta* **74**, 5259–5279.

Wimpenny J., James R. H., Burton K. W., Gannoun A., Mokadem F. and Gíslason S. R. (2010b) Glacial effects on weathering processes: new insights from the elemental and lithium isotopic composition of West Greenland rivers. *Earth Planet. Sci. Lett.* **290**, 427–437.

Wronkiewicz D. J. and Condie K. C. (1987) Geochemistry of Archean shales from the Witwatersrand supergroup, South Africa source area weathering and provenance. *Geochim. Cosmochim. Acta* **51**, 2401–2416.

Wu F. Y., Sun D. Y., Li H. M., Jahn B. M. and Wilde S. (2002) A-type granites in northeastern China: age and geochemical constraints on their petrogenesis. *Chem. Geol.* **187**, 143–173.

Yang J. H., Wu F. Y., Chung S. L., Wilde S. A. and Chu M. F. (2004) Multiple sources for the origin of granites: geochemical and Nd/Sr isotopic evidence from the Gudaoling granite and its mafic enclaves, northeast China. *Geochim. Cosmochim. Acta* **68**, 4469–4483.

Yang J. H., Wu F. Y., Chung S. L., Wilde S. A. and Chu M. F. (2006) A hybrid origin for the Qianshan A-type granite, northeast China: geochemical and Sr-Nd-Hf isotopic evidence. *Lithos* **89**, 89–106.

You C. F. and Chan L.-H. (1996) Precise determination of lithium isotopic composition in low concentration natural samples. *Geochim. Cosmochim. Acta* **60**, 909–915.

Young G. M., Brunn Von., Gold D. J. C. and Minter W. E. L. (1998) Earth's oldest reported glaciation: physical and chemical evidence from the Archean Mozaan Group (~2.9 Ga) of South Africa. *J. Geol.* **106**, 523–538.

Zahnle K. and Sleep N. H. (2002) Carbon dioxide cycling through the mantle and implications for the climate of ancient Earth. In *The Early Earth: Physical Chemical and Biological Development, Vol. 199* (ed. C. Fowler). Geological Society of London, Special Publication, pp. 231–257.

Zhou C. M., Tucker R., Xiao S., Peng Z., Yuan X. and Chen Z. (2004) New constraints on the ages of Neoproterozoic glaciations in south China. *Geology* **32**, 437–440.

Associate editor: Brian W. Stewart